UNIVERSITY OF PADOVA

Department of Information Engineering

Master Degree in ICT for Internet and Multimedia

A simulation study of beam management for 5G millimeter-wave cellular networks

SUPERVISOR
Prof. Michele Zorzi

CANDIDATE
Luca Dalla Gassa

CO-SUPERVISORS
Prof. Marco Giordani
Matteo Pagin

Date: 12/12/2022

A.Y.: 2021/2022

Abstract

The 5th generation (5G) of mobile networks will be required to sustain the rapidly increasing number of mobile devices, voluminous data, and broadband services. The introduction of millimeter wave bands communications promises to partially solve these challenges, since this technology exploits a new portion of the spectrum that can provide unprecedented data rates to next-generation cellular mobile terminals. However, millimeter wave links are plagued by a higher free-space path loss, compared to sub-6 GHz bands, and are susceptible to rapid channel variations. These harsh propagation conditions can be overcome by using beamforming to focus the transmission power towards the intended receiver. In turn, this introduces the need for the alignment of the transmitter and the receiver beams, which involves important implication for the control layer procedures such the initial access, handover and beam tracking.

For this reason, in this thesis we aim at studying a realistic downlink-based beam management procedure based on the Synchronization Signal Block, with different configurations implemented in the discrete-event network simulator ns-3. We compare the network performance achieved by these configurations via a full-stack simulation campaign.

Contents

Chapter 1

Introduction

In recent years, the demand of high-performance wireless communication is increasing, becoming crucial for many aspects as the digital transformation of industrial systems or the daily life of any user. Fifth-generation (5G) technology is built to meet new communication requirements as low-latency, high data rate, and high-reliability connections among mobile devices [1]. More specifically, these values are set by "International Mobile Telecommunications-2020" (IMT-2020 Standard) for 5G networks and services [2]. In Fig.1.1 it is possible to observe these requirements, and the differences between 4G and 5G technologies.

The need for extreme data rate is driven by the use of better devices, better user interface design, involving services (e.g., video streaming), and the need to be high-speed connected anywhere and anytime. This is possible increasing the bandwidth and using different modulation and coding schemes. It should be pointed out that, in current cellular systems, it is not only mobile data traffic that is dramatically increasing, considering that signaling traffic is increasing 50 % faster than data traffic [3].

Moreover, cellular networks are not just asked to support mobile users traffic anymore. Indeed, the ever-increasing number of IoT devices, such as smart wearable devices, smart household appliances,

	4G	5G
Time delay	10 ms	smaller than 1 ms
Number of mobile links	eight billion	eleven billion
Channel broadband	20 MHz 200 MHz	100 MHz (lower than 6 GHz) 400 MHz (larger than 6 GHz)
Frequency band	600 MHz to 5.925 GHz	600 MHz (millimeter wave)
Date flow	7.2 Eb/month	50 Eb/month
Peak data rate	1 Gb/s	20 Gb/s
Available channel	3 GHz	30 GHz
Link density	One million links/km*2	One million links/km*2
Uplink waveform	Use SC-FDMA	Use CP-OFDM

Figure 1.1: Comparing 4G and 5G[4]

autonomous cars, sensors and mobile objects like drones, incurs an additional, novel burden on current and future cellular networks. In particular the 5G technology allows to deploy a large number of sensors in the framework of IoT and to process massive data. The most commonly used methods and technologies in 5G IoT to analyze and process the huge amount of data are deep learning, reinforcement learning and big data miming [5]. The architecture of the 5G - IoT can be seen in Fig.1.2

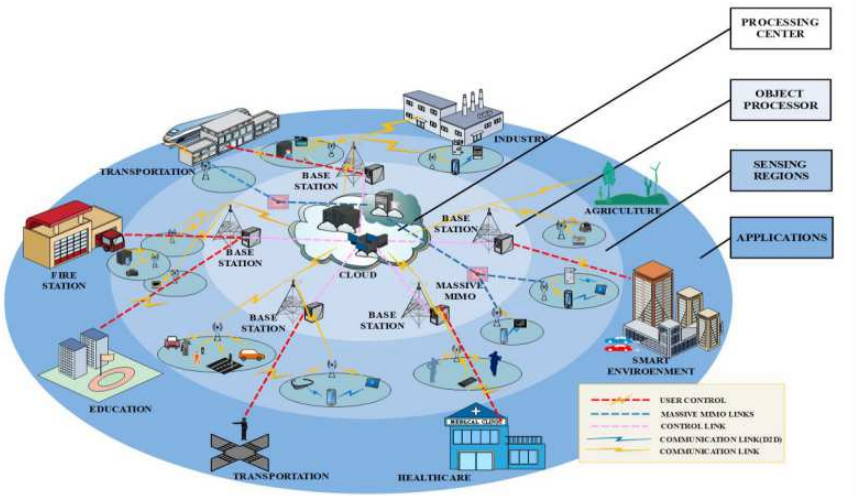

Figure 1.2: The architecture of the 5G-IoT[5]

With regards to the throughput requirements set in IMT-2020, the major technology enabler is represented by the so called mmWaves, which refers to the portion of the electromagnetic spectrum which spans approximately from 10 to 100 GHz. MmWaves offer a huge amount of untapped bandwidth, which in turn offer the potential for Gbit/s data rates, however, these frequencies exhibit unfavorable propagation characteristics [6]. In particular, compared to sub-6 GHz bands, mmWaves are characterized by higher omnidirectional propagation pathloss, rain and foliage-induced attenuation [7] and increased susceptibility to blockages due to obstacles. These phenomena can be partially mitigated by exploiting the properties of mmWaves antennas. Indeed, at these frequencies it is possible to pack an high number of antenna element thus achieving high beamforming gain, thanks to the smaller size of the radiating elements, when compared to sub-6 GHz antenna devices. Moreover, mmWaves antennas exhibit an intrinsic higher directivity as well. The set of operations that enable the fine alignment of the transmitter and receiver beams are known as beam management, and they are crucial to perform some control tasks as Initial Access (IA) and beam tracking. The IA procedure allows the user to establish a physical connection with the gNB the first

time it accesses the network, while beam tracking regards connected users, and enables beam adaptation schemes and recovery procedures in case of radio link failures and/or mobility [8].

This thesis is based on 3GPP standard (3rd Generation Partnership Project), which combines seven telecommunications standard development organizations (ARIB, ATIS, CCSA, ETSI, TSDSI, TTA, TTC) and standardizes the specifications to provide a stable environment in which define new technologies. The project meets cellular telecommunications technologies as radio access and core network but it faces also with non-radio access and interworking with non-3GPP networks [9].

In order to implement the 3GPP NR beam management procedure ns-3 is used, a discrete-event network simulator for TCP/IP systems. Ns-3 is an open-source software, licensed under the GNU GPLv2 license, and maintained by a worldwide community [10].

This thesis aims at performing a system-level analysis of beam management protocol under different scenarios, mobility conditions and parameters configurations. In particular, compared to the actual state of art, this work implements a realistic downlink-based beam management procedure based on the SS blocks, with end-to-end metrics and full-stack simulator. The goal is to analyze the PHY layer performance measured in terms of SNR, and the impact on the application level by inspecting latency, throughput, and packet drop rate.

More specifically, the thesis is organized as follows:

- chapter 2 describes the architecture and overall design of a 5G cellular network, with particular focus on the beam management procedures;
- chapter 3 explains the mmWaves spectrum and its propagation characteristics;
- chapter 4 describes the baseline ns-3 simulator and the changes

which have been introduced to implement a realistic beam management procedure;

- chapter 5 presents the simulation scenarios and parameters and provides a thorough analysis of the obtained results;
- chapter 6 concludes this thesis by summing up its main contributions and outlining possible future extensions of this work..

Chapter 2

5G characteristics and applications

This chapter provides an overview of the essentials of the state of the art in 5G technology represented by the 3GPP technical specifications, with a focus on the most important proposed technologies for the deployment of 5G networks. The fundamental concepts which will be explored are the new radio access technology, where are explained the frame structure, the scheduling and the transmission of the data, and the Initial Access (IA) procedure. In the second part of the Chapter will be introduced the so called mmWaves, which investigate a new portion of the spectrum, and their features, such as the propagation loss and the directivity.

2.1 Basic overview

During the last 30 years, technology progress has led to progressively improved communications systems. This process began with the first generation (1G), which refers to the non-cable telecommunication technology, where devices are known as "cellphones". In the early 90s was introduced the second generation (2G) wireless cellular networks. In this step was introduced data exchange [11], where it is not possible transfer data such as mail or software but rather voice and other data basic aids [12].

Third generation (3G) enables operators to provide users with ser-

vices while reaching greater network capacity through an improved spectrum efficiency [12]. Moreover 3G improved security features, building a flexible architecture which was easily adaptable in the following technologies.

Then, in March 2009, the International Telecommunications Union-Radio (ITU-R) drafted the requirements for fourth generation (4G) systems. The main targets were peak speed requirements for high and low mobility communications. In the first case, such as trains and cars, the peak speed requirements is 100 Mbs, while for low mobility communications, involving pedestrians and stationary users, is 1 Gbs [11]. The era of 3G and 4G networks had an important scientific progress in micro and power electronics, in particular in minimizing the dimensions of the hardware [11]. This step was relevant and posed the way for the development of advanced transceiver architectures that support large bandwidths and multiple Radio Frequency(RF) chains. In this context was introduced the MIMO (Multiple Input Multiple Output), a transmission technique studied over the years that is related to the use of multiple antenna elements at both the transmitter and the receiver.

Although MIMO systems were incorporated in 3G and 4G standards, the increasing demand for higher data rates and better performances, led the industry to search for new solutions that include additional bandwidth [11]. In particular, looking at the evolution of mobile communication systems, can be easily observed that companies are trying to reach a compromise between the increasing user needs and the development of technologies able to satisfy the requirements given the scarce spectrum. In this context the most important proposed technologies for the deployment of 5G networks are a new radio access technology, mmWaves, and massive MIMO.

2.2 New radio access technology

From 2020, the 5G standard is going to progressively replace the previously used 4G technology, aiming to solve its problematic aspects, and meeting the new performance requirements dictated by the current technological advances.

New Radio (NR), i.e., the Radio Access Network of 5G systems, is a turning point for wireless communication. The three main novel use cases defined by the International Telecommunication Unit (ITU) are: Enhanced Mobile BroadBand (eMBB), Ultra-Reliable Low Latency Communications (URLLC), and Massive Machine-Type Communications (mMTC) [1]. In Fig.2.1 and 2.2 are presented the basic features for eMBB, URLLC and mMTC.

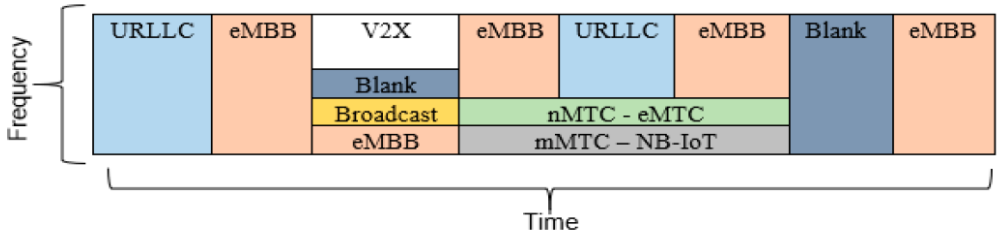

Figure 2.1: The flexible frame structure of 5G new radio(NR) [1]

Category	Basic Features
eMBB	eMBB focuses on a higher data rate, with a large payload and prolonged internet connectivity based applications. Potential applications could include cloud office/gaming, virtual/augmented reality (VR/AR) and three-dimension/ultra-high-definition (3D/UHD) video.
URLLC	URLLC focuses on an ultra-responsive connection with ultra-low latency. The data rate is not expected to be very high in URLLC, but offers high mobility. Potential applications of URLLC include industrial automation, autonomous driving, mission-critical applications, and remote medical assistance.
mMTC	mMTC focus on providing connectivity to a large number of devices (IoTs), but with low reliability. It can provide long-range communication with energy efficiency and asynchronous access. Such features are very suitable for low power devices in a massive quantity.

Figure 2.2: Basic features [1]

NR introduces several novelty with respect to previous generations,

especially new degrees of freedom and flexibility in the management and configuration of the network. Considering the rapid technology changes, NR is designed not only to provide the three categories defined by ITU, but also to support possible future adjustments as shown in Fig.2.3.

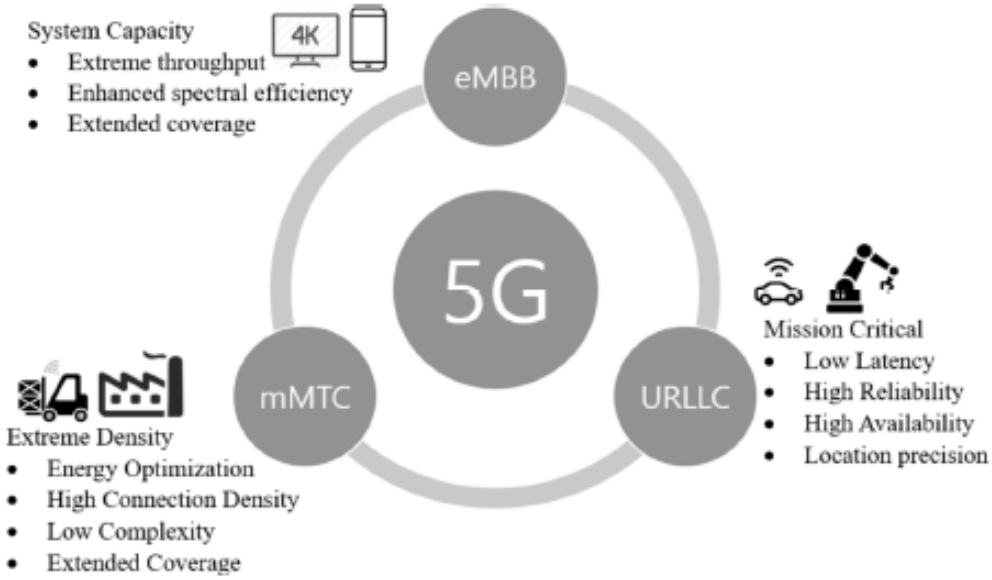

Figure 2.3: Features and improvement plan for future 5G [1]

Moreover, 5G NR is characterized by specific features such as ultra-lean design principle, transmission scheme and frame structure, the duplex schemes, scheduling and data transmission, and IA.

2.2.1 Ultra-lean design principle

In the mobile communication system some signals are named 'always on' signals, e.g., broadcast signals, reference signals, and synchronization signals. These signals are transmitted after a regular interval of time even if user has no data for transmission. The 5G standard has pushed towards an ultra-lean design, with the goal of minimizing the always on transmissions and promote energy efficiency. The adoption of ultra-lean design principle enables higher network energy performance and higher achievable data rates. This is possible by

transmitting four primary reference signals like Phase Tracking Reference Signals (PTRS), Channel State Reference Signals (CSI-RS), Sounding Reference Signals (SRS), and Demodulation Reference Signals (DMRS), only when it is required [13].

2.2.2 Frame structure

In order to support different scenarios and deployments, NR supports a flexible numerology, as described in Table 2.1. Time resources are subdivided into radio frames, the duration of which is 10 ms, with 10 subframes of 1 ms, while each slot is composed of 14 OFDM symbols. Unlike in 4G and previous generations, the number of slots in the subframe depends on the numerology, since the symbol duration is inversely proportional to the subcarrier spacing, which ranges from 15 kHz up to 240 kHz. NR Frame Structure supports both Frequency Division Duplexing (FDD) and Time Division Duplexing (TDD), while the waveform is OFDM with a cyclic prefix [8]. Looking at the time and frequency domain, the frame structure of NR is similar to that of LTE, with a higher number of configurable parameters. In Release 15 are admitted at most 3300 subcarriers, for a maximum bandwidth of 400 MHz. Fig.2.4 shows NR time-domain structure, where is also visible the position of downlink and uplink control signals, respectively represented by the first and the last symbol in the slot.

Numerology index\μ	Number of symbols per slot	Number of slot per frame	Number of slot per subframe	Subcarrier spacing
0	14	10	1	15 kHz
1	14	20	2	30 kHz
2	14	40	4	60 kHz
3	14	80	8	120 kHz
4	14	160	16	240 kHz

Table 2.1: 5G NR numerologies and corresponding number of symbols per slot, slot per subframe, slot per frame, and subcarrier spacing.

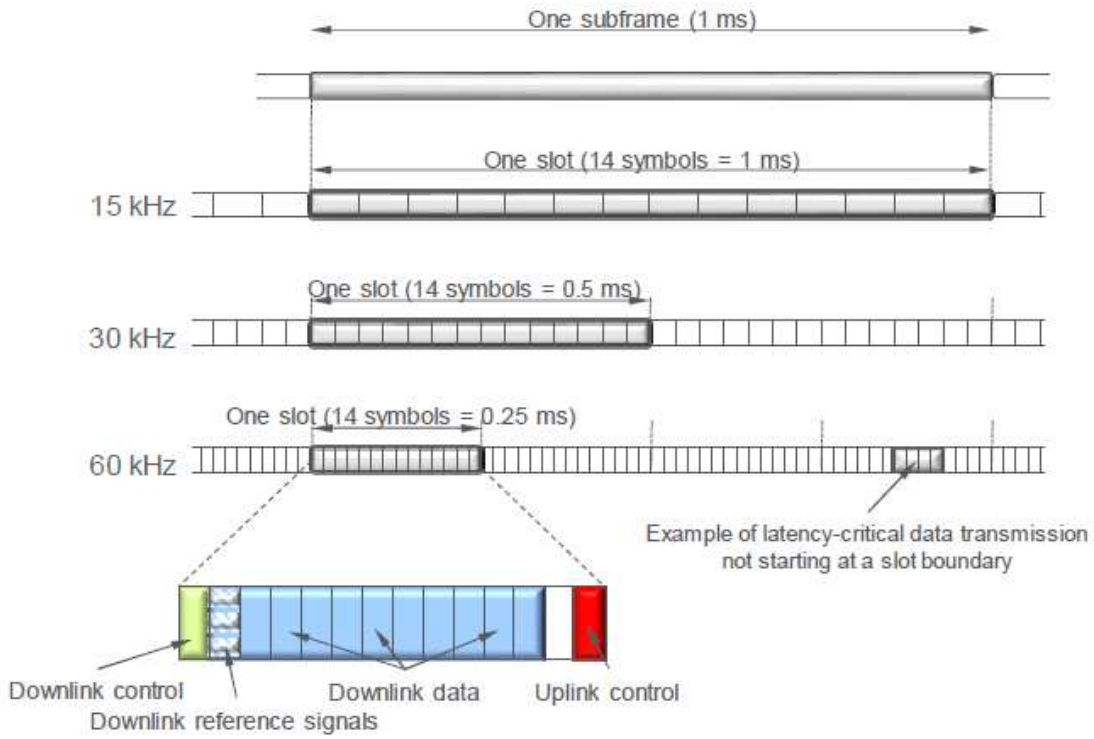

Figure 2.4: NR time-domain structure [14]

2.2.3 Duplex schemes

In contrast to LTE, NR can operate in both paired and unpaired spectrum using a common frame structure. The basic frame structure can support both half-duplex and full-duplex operations. In the first case the device cannot transmit and receive at the same time while in full-duplex operation is possible. Moreover NR supports *dynamic TDD* to meet rapid variations in dense deployment with small cell sizes. With this technologies the time resources can be dynamically assigned to downlink or uplink transmission, depending on the traffic [14].

2.2.4 Scheduling and data transmission

The NR scheduling framework is similar to the LTE. Scheduling decisions are taken by a scheduler, which resides in the base station (BS).

The time and frequency resources allocations are taken based on the Buffer Status Reporting (BSR) and the channel quality reports done by the user.

Each device can control a number of physical downlink control channels (PDCCH), once per slot although it is possible to configure more frequent monitoring to support traffic requiring very low latency.

In the downlink transmissions PDCCH is used for dynamic scheduling to deliver Downlink Control Information (DCI), which includes information required by the user to schedule data [15]. Consequently, in the uplink transmissions, the user reports its Hybrid ARQ acknowledgement (HARQ-ACK) feedback through the the physical uplink control channel (PUCCH). The HARQ is used from the user to report the outcome of the decoding operation to the BS, which asks for retransmission if it fails to decode the uplink data. Thereby the uplink transmissions are only used to refer any kind of issues in the decoding operation.

A key difference from LTE is the highly symmetric properties between downlink and uplink scheduling. In LTE the radio resource allocation schemes are different between downlink and uplink transmissions due to different multi access schemes, while in NR scheduling mechanisms such as radio resource allocation, rank/modulation/coding adaptation and adaptive Hybrid ARQ are common between downlink and uplink [15].

2.2.5 Initial Access

IA is a procedure by which a device finds a cell to connect with and requires time and frequency synchronization. The basic structure of NR IA is similar to the corresponding LTE, with a Primary Synchronization Signal (PSS) and a Secondary Synchronization Signal (SSS) used to find, synchronize to and identify a network. In light of the lean design principle and due to the absence of frequent static ref-

erence signals to aid tracking, there could be larger initial frequency errors between the BS and the user compared to LTE [16]. To solve the problem is used a BPSK modulated m-sequence of length 127 [16]. Therefore, PSS and SSS can identify 1008 different cell identities, twice as many as that of LTE [15].

The Physical Broadcast Channel (PBCH) detects the Master Information Block (MIB) of a cell, and enables reception of PDCCH and Physical Downlink Shared Channels (PDSCH) [15]. PSS, SSS, and PBCH consitute the Synchronization Signal Block (SSB).

There are some other differences between LTE and NR. In order to reach higher energy performance, and in view of the flexibility feature of NR, the SS blocks are transmitted in a localized burst with set periodicity (default at 20 ms), while the corresponding signal in LTE is transmitted every 5 ms [14]. In Fig.2.5 is shown the group of 4 OFDM symbols that represent the time composition of SSB, and 240 contiguous subcarriers (20 Resource Blocks) in frequency [16]. In particular, the subcarrier spacings considered for IA at frequencies above 6 GHz are 120 and 240 kHz, i.e, 15 x 2^n kHz, with $n \in$ [3,4].

Considering a single burst, it can be transmitted up to 64 SSB, and the transmission is confined to a 5 ms window. The set of possible SSB time locations within the frame depends on the numerology, identified by the frequency band.

The last key feature that characterizes the NR access is the expansion of the range of spectrum in which the radio-access technology can be deployed, that is mmWaves bands.

2.3 MmWaves

Due to the extremely crowded nature of below 6 GHz bands, during the last 10 years there have been significant research efforts on considering new portions of the spectrum. In particular, most efforts

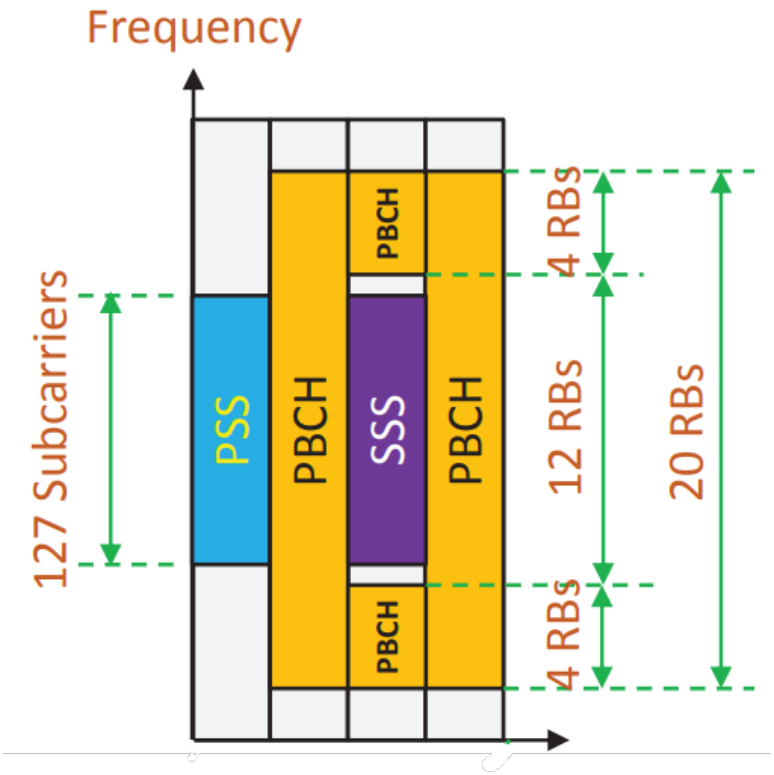

Figure 2.5: SSB structure [8]

focused on the so called mmWaves, which loosely span from 10 to 300 GHz and currently play a key role in meeting the multi-gigabit communication requirements.

Because of huge bandwidth, mmWaves small cells are able to provide gigabit-per-second rates, wideband multimedia applications such as high-speed data transfer between devices, real time streaming, wireless gigabit Ethernet and wireless gaming.

The differences with legacy communication systems operating in the sub-6 GHz bands as 2.4 and 5 GHz, call for an adaptation of the physical layer (PHY), the medium access control (MAC) and upper layer [17]. In particular, mmWaves come with several issues in terms of propagation, including severe path loss, directivity, sensitivity to blockage and dynamics due to mobility, as described in the following subsections.

2.3.1 Propagation loss

Compared to other portions of the spectrum, mmWaves suffer from huge propagation loss. Furthermore, mmWaves are subject to additional attenuation factors compared to sub-6 GHz, such as rain, atmospheric and molecular absorption, foliage, and also snow or fog, and these factors vary according to band [17]. For example, the atmospheric attenuation at 28, 38 and 73 GHz are respectively 0.012, 0.016, and 0.060 dB. These evaluations are done in a bounded area (200 m) in an outdoor urban environment. Looking instead the frequency band at 60 GHz, the atmospheric attenuation is around 4 dB, therefore the results are more pronounced [18]. Fig.2.6 shows the atmospheric absorption at mmWave frequencies, where oxygen absorption in the 60 GHz band has a peak, ranging from 15 to 30 dB/km [17].

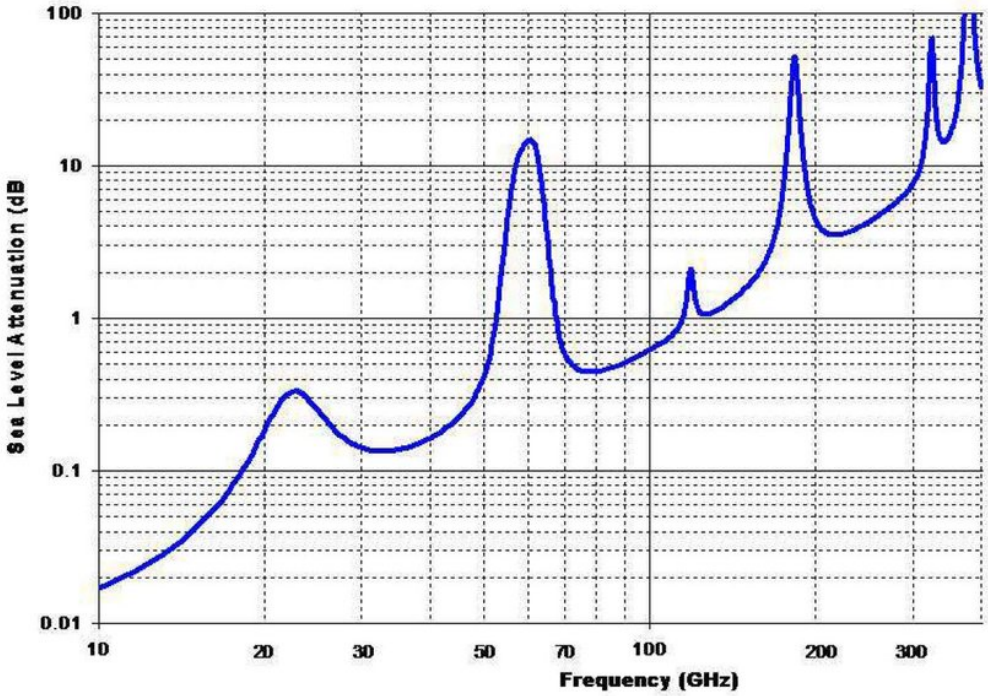

Figure 2.6: Atmospheric and molecular absorption at mmWave frequencies [17]

Regarding instead rain attenuation, a possible issue is given by the raindrops, which have comparable dimension of radio wavelengths at mmWave frequencies. This can induce scattering of the radio signal

[19]. However, by using smaller cell sizes in the order of 200 m, both rain attenuation and atmospheric absorption can be limited. Rain can be classified into four different categories according to rainfall rate [18]:

- light rain refers to rainfall of 0.25-1.00 mm per hour;
- moderate rain refers to rainfall of 1-4 mm per hour;
- heavy rain refers to rainfall of 4-16 mm per hour;
- very heavy rain refers to rainfall of 16-50 mm per hour;

In Fig.2.7 it is possible to observe the rain attenuation in different situations, measured in dB/km. Taking into consideration the "very heavy rain" case, for example 25 mm/hr, the rain attenuation at 28 GHz and 73 GHz is around 7 dB/km and 10 dB/km. This means that even in the case of heavy rainfall, considering a cell range in the order of 200 m in radius, the value of rain attenuation is reduced to only 1.4 dB at 28 GHz and 2 dB at 73 GHz [17].

The last attenuation factor which has an impact at mmWaves is foliage losses, which are significant and can affect, as rain, the network performance. These losses can be described as follows:

$$\gamma = 0.2(f)^{0.3}(R)^{0.6} \tag{2.1}$$

where R is the depth of the foliage in meters and f is the frequency in MHz [20].

2.3.2 Directivity

Thanks to the small wavelength it is possible to realize large-scale steerable antenna arrays as patterns of metal on circuit boards [17]. In fact, by controlling the phase of the signal transmitted by each

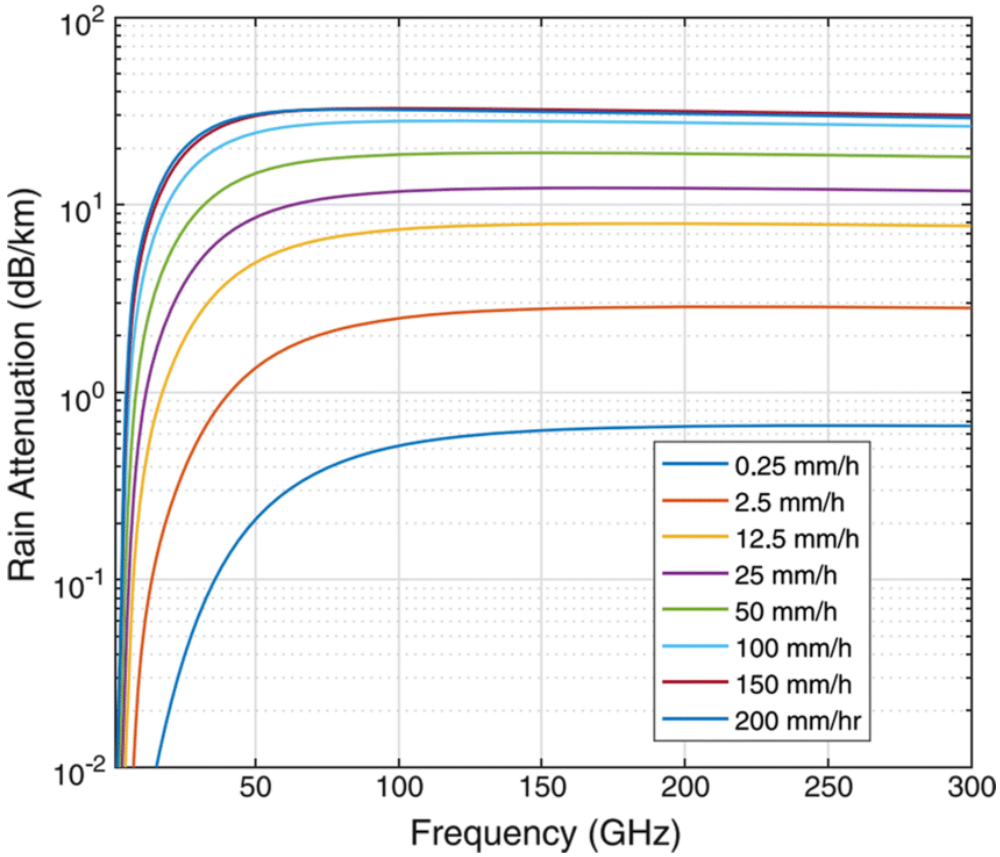

Figure 2.7: Rain attenuation measured in dB/km at different rainfall rates [18]

antenna element, the antenna array can steer beams towards any direction achieving antenna gains by beamforming, which can partially compensate for the increased path loss experienced at mmWave frequencies. However, this in turn creates the need for an alignment between the transmitting and receiving beams, which is possible through the procedure of beam training, as described in Chapter 3.

2.3.3 Sensitivity to blockage

Generally speaking, electromagnetic waves do not diffract around the obstacles whose size is significantly larger than the wavelength. At mmWaves, instead, signals are susceptible to blockages due to obstacles such as people and furniture [21]. For example, the authors of [22] show that human blockage attenuates the link budget by 20-30 dB.

Another work done by Collonge et al. [23] in a realistic indoor environment with human activity demonstrates that the channel is blocked for about 1 or 2 % of the time due to the presence of one to five persons already. This phenomenon is sufficient to render mmWaves links intermittent, possibly representing a critical problem for delay-sensitive applications and a big challenge for mmWaves communications.

To ensure a reliable network connectivity were proposed different approaches from physical layer to network layer. A possible approach is to exploit reflections from walls and other surfaces to steer around the obstacles [24]. A different method is switching from a Line Of Sight (LoS) link to a Non Line Of Sight (NLoS) link (NLoS link are significantly attenuated and cannot support high data rate), as described in [25] and [26]. In particular the last paper presents a scenario, depicted in Fig.2.8, where there are three buildings between the BS, which has 64 antennas, and the user, characterized by 16 antennas.

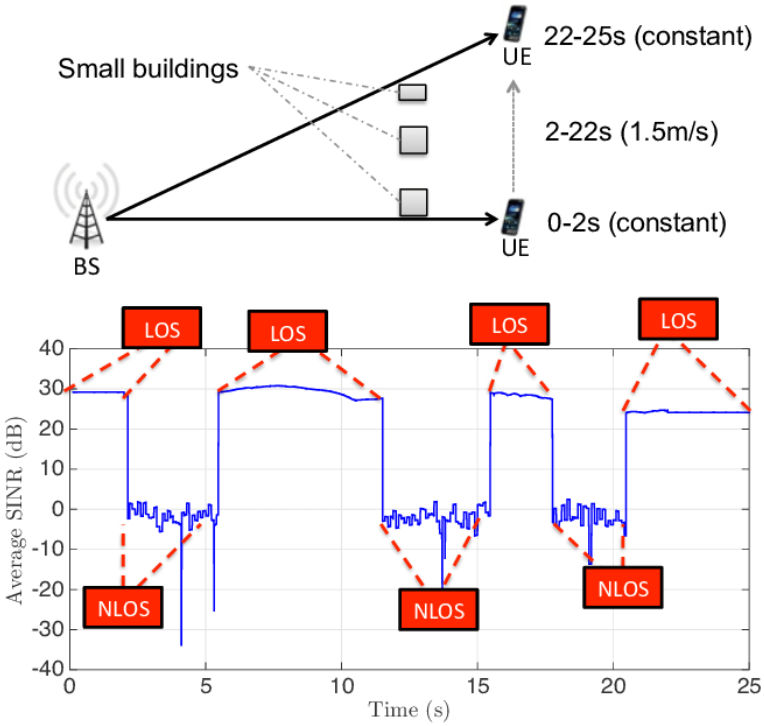

Figure 2.8: Example of solution based on the switch from LoS link to NLoS and viceversa [26].

The user moves at a speed of 1.5 m/s 2 seconds after the start of the simulation and stops after 20 seconds. As expected, when the user does not move (0-2 s and 22-25 s), the SINR is constant. However, the variations of the SINR when the user is in motion result from the switching from NLoS to LoS channel and viceversa.

Finally, another model to ensure a reliable network connectivity is proposed in [27], in which is explored a spatial diversity technique, where multiple beams are formed at the same moment during a beamforming process. The pro is to maintain a reliable connectivity if obstacles block the strongest path, the cons is the overhead of the beamforming process which can degrade the performance of the system.

Chapter 3

Beam management in 5G NR and MIMO limitation

At the beginning of this Chapter will be analyzed the beamformer basics, where are introduced the concepts and the structures that characterize the beamforming antennas. Consequently, the architecture of the beamforming, i.e., analog, hybrid, and digital beamforming, is explored. In the second part of the Chapter will be explained the beam management procedures, distinguishing in particolar between the idle mode beam management and the connected mode beam management.

3.1 Basic overview

Beamforming antennas are an essential tool for mobile operators as they build out their networks for capacity and 5G NR. Unlike traditional antennas which transmit and receive only on fixed radiation patterns, beamforming antennas can dynamically shape the transmitting direction based on the location of the connected user, as depicted in Fig.3.1. This is possible through a signal processing technique which automatically adjusts the incoming signal from collected information and weight [28].

Beamforming antennas have multiple benefits, such as the reduction of interference, a better end user experience, an improvement

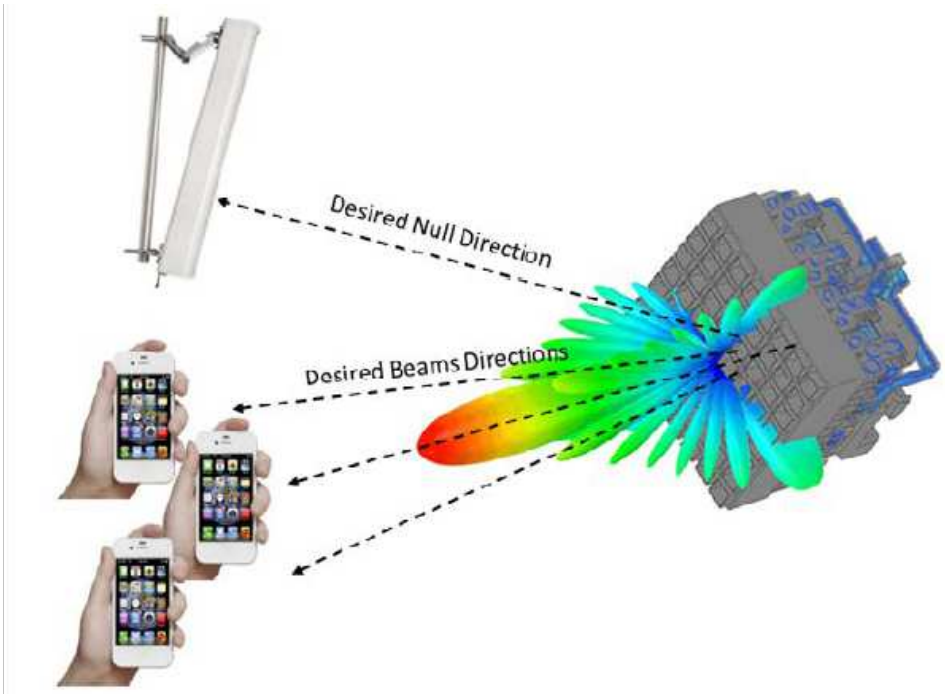

Figure 3.1: The beamforming technique makes beam toward the signal of interest and produce null toward the direction of signals not of interest[28]

of signal-to-interference-and-noise ratio (SINR) [29], and they have a specific configuration according to the environment to which they are intended. The beamformers' design share three main aspects:

- they contain active or passive antennas. Passive antennas are built entirely out of passive elements, while active antenna systems contain active components, which allow the control of the antenna performance in order to maintain the best possible operation for any conditions;

- they use analog, hybrid or digital beamforming, explained in Section 3.4;

3.2 Beamformer basics

Advanced antennas are the crucial aspect to enable beamforming capabilities. We introduce the following concepts.

- **Phased arrays beamforming:** as depicted in Fig.3.2 when multiple antenna elements (AE) are installed and aligned in a shared reflector, it is created a panel antenna arrays;

Figure 3.2: Panel antenna linear array [29]

- **Antenna elements:** The most common types of AE are wire, e.g. dipole and monopole elements, and aperture elements, such as slot elements. Some designs include combinations of both types;

- **Antenna array patterns:** Each AE has its own radiation pattern while the RF effect depends on the array size and element spacing, the amplitude variation, and the elements' signal phase shifts. The combination of these variables, which describe the array factor pattern, and the element pattern, produces the overall far field radiation pattern of the panel antenna;

- **Antenna gain:** The maximum directivity is obtained setting the spacing of the elements to $\lambda/2$, where λ is the wavelength. At the gNB, i.e., the 5G radio network node, a single sector can be divided in three sector site: the azimuth θ varies from -60 to 60 degrees, the elevation ϕ varies from -30 to 30 degrees, and a fixed mechanical tilt of the array pointing towards the ground [8]. As depicted in Fig. 3.3, there is a strong correlation between

beamwidth, number of antenna elements, and beamforming gain, since narrower beams means higher beamforming gain, and more directional transmissions.

The antenna gain is equal to its directivity in a lossless array, which can be expressed as[29]:

$$Antennagain(dB) = Elementgain + 10log_{10}(N) \tag{3.1}$$

where N is equal to the number of array elements, and element gain is the gain of a single radiator embedded in the array, or

$$Antennagain(dB) = Elementgain + 3log_{2}(N) \tag{3.2}$$

.

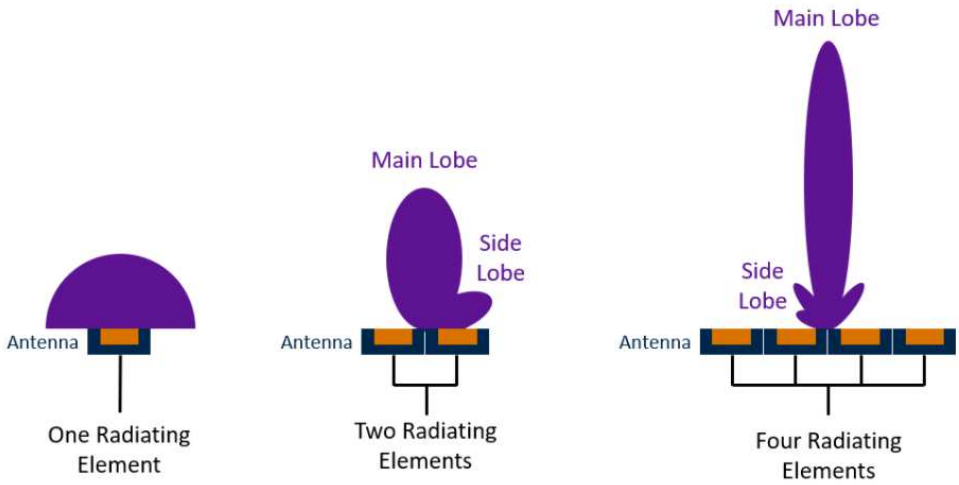

Figure 3.3: Beamforming with one, two and four radiating elements [30]

- **Element spacing effect:** the antenna element spacing determines the shape and the gain of the pattern. Fig.3.4 represents a four-element array in which is increased the spacing from 0.5λ to

2λ, increasing the main lobe gain but also generating sidelobes which disperse the radiated power of the main lobe;

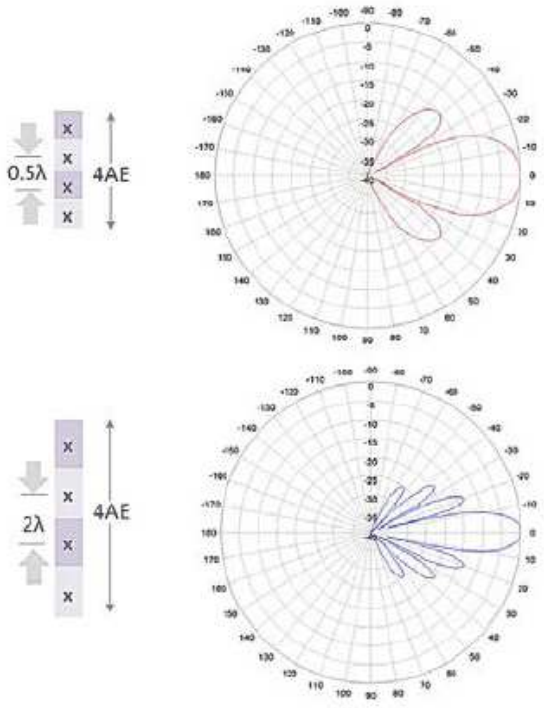

Figure 3.4: Antenna elements spacing effect [29]

- **Phase shift effect:** Even though the number of antenna elements and their spacing is fixed for each antenna in the phased array, by controlling the RF signal phases and amplitudes it is possible to shape the overall radiated pattern. In fact, in-phase waves can be added constructively, while out-of-phase waves work destructively.

3.3 Beamforming architecture

Three different beamforming architecture can be applied both at the UE and at the gNB.

Analog beamforming employs only a single RF chain to support large antenna arrays and performs the beamforming via low-cost phase-shifters at the RF-stage [31]. In the analog beamforming model, the

transmission can be done in only one direction at any given time, therefore the flexibility is low. On the other hand this model allows to save power since a single pair of Analog to Digital Converter (ADC) is used. Fig.3.5 represents the analog beamforming model, where a single RF source is split among multiple antenna elements and the beam can be controlled by adjusting the analog phase shifters.

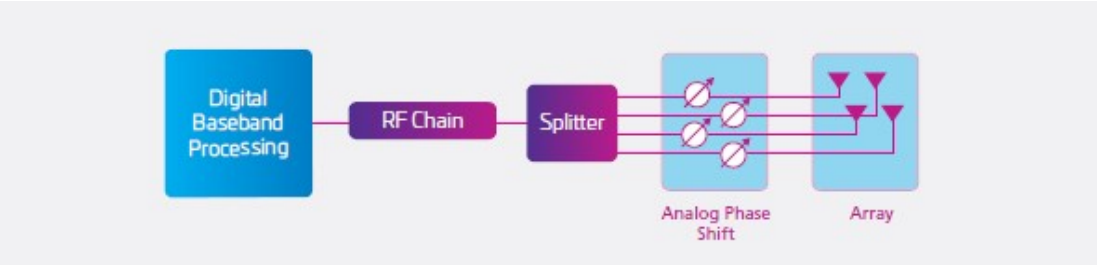

Figure 3.5: Analog beamforming [29]

Hybrid beamforming uses $K_{BF} \leq N$ (i.e. N represents the number of antenna elements) RF chains in order to represent K_{BF} parallel analog beams. The transceiver can transmit and receive in K_{BF} different direction simultaneously, therefore this mechanism reduces the received power at each transmitting beam since the total node power is divided by K_{BF}. Fig.3.6 depicts a hybrid beamforming model, where RF chains and splitters are digitally controlled, while phase shifters are set analogically.

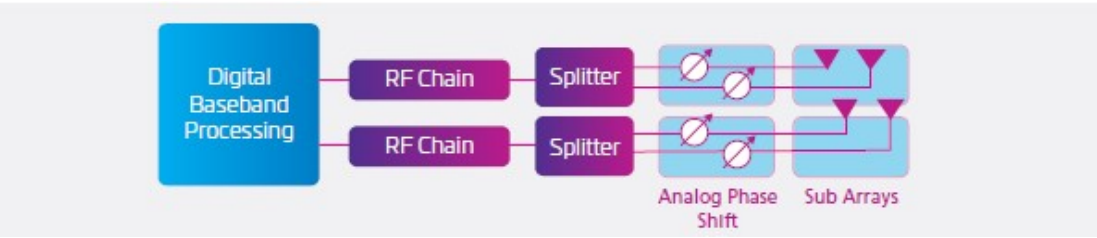

Figure 3.6: Hybrid beamforming [29]

Digital beamforming requires a dedicated RF chain and data converter for each antenna element, therefore each signal can be processed in the digital domain. In this model the transceiver is potentially able to direct beams in infinitely many directions, since the

transceiver can apply a weight to the received signals enabling more powerful and flexible processing than that in the analog domain. As in the hybrid beamforming model, the possibility to transmit multiple beams in different directions simultaneously involves a reduced transmit power being available to each. Digital transceiver can process at most N orthogonal beams simultaneously, therefore the number of parallel beams that can be generated is limited to N. Moreover, to avoid higher energy consumption in transmission, the digital beamforming model is implemented only at the receiver side [8].

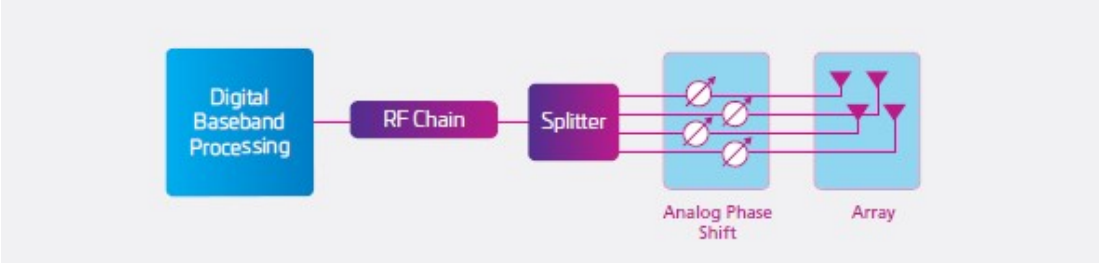

Figure 3.7: Digital beamforming [29]

3.4 Limitation of MIMO

The improvements resulting from the use of MIMO are clear, but this technology presents also some issues that have to be addressed. The first one is the performance degradation due to hardware impairments in case low-cost RF chains are used in the system [32]. Actually, a large number of antennas means increasing the costs for the components, therefore to avoid this scenario are often implemented non optimal elements, such as low resolution ADC, which can be implemented with simple circuits.

Channel estimation errors and channel aging effects represent another problem which can deteriorate the system performance, especially in high-speed environments.

The high throughput caused by the use of a large number of antennas allows more users to communicate simultaneously at the same

time-frequency resource, but for large antenna arrays the signal processing technique becomes demanding due to the high signal dimensions. Therefore it becomes essential to allow this multiplexing gain with low-complexity signal processing and basic hardware implementations.

Under certain circumstances performance of a large array becomes limited by interference arising from re-use of pilots in neighboring cells[32]. Pilot contamination, which represents a critical problem for Massive MIMO technology, is caused by the lack of orthogonality in pilot sequences transmitted from adjacent cells, since they create additional interference in the uplink during training stage and in the downlink during the data transmission stage. The problem of pilot contamination is depicted in Fig.3.8, where the solid line represents the direct gain and the dotted line represents the inter-cell interference.

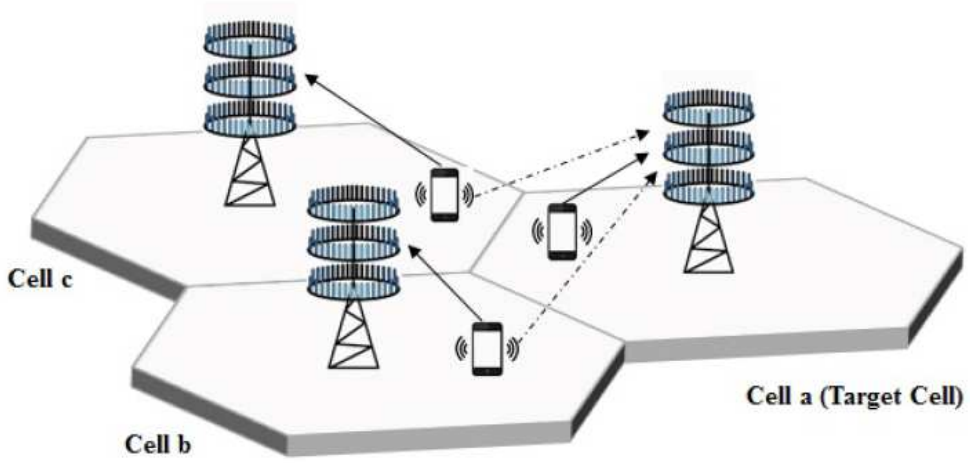

Figure 3.8: The effect of pilot contamination in multicell massive MIMO systems at a cell a [33]

3.5 Beam management procedure

In order to support directional communications, the 5G NR specifications include a new set of operations, known as beam management,

to perform a variety of control tasks including the IA for idle users, which allows a mobile user to establish a physical link connection with a gNB, and beam tracking for connected users, which enables beam adaptation schemes, or path selection and radio link failure recovery procedures. The procedures of beam management include four different operations [8]:

- **Beam sweeping:** The radiating pattern covers a spatial area, using a multi-directional beam sweep and pre-specified time intervals.
- **Beam measurement:** The quality of the received signal at the 5G NodeB or the user is evaluated.
- **Beam determination:** the selection of the suitable beam or beams either at the gNB or at the UE, according to the measurements obtained with the beam measurement procedure..
- **Beam reporting:** User's feedback on beam quality and decision information to the RAN.

These procedures need to be periodically repeated to update the optimal transmitter and receiver beam pair over time.

3.5.1 Idle mode beam management

The idle user establishes a directional physical link connection through the IA procedure. The role of the downlink SS, introduced in Section 2.2.5 is essential for the IA procedure, thereby 3GPP defines a directional version of it for 5G NR. In a slot of 14 OFDM symbols, the SS block can be placed in two different locations: symbols 2-5 and symbols 8-11 [8]. Each SS block during beam operations, is mapped to a certain angular direction, as shown in Fig.3.9, enabling the gNB, to cover a whole cell sectors by sequentially sweeping different angular directions, i.e., beam sweeping phase. To reduce the effect of

SS transmissions, SS blocks can be sent through wide beams, at the expense of reducing the beamforming gain. [34].

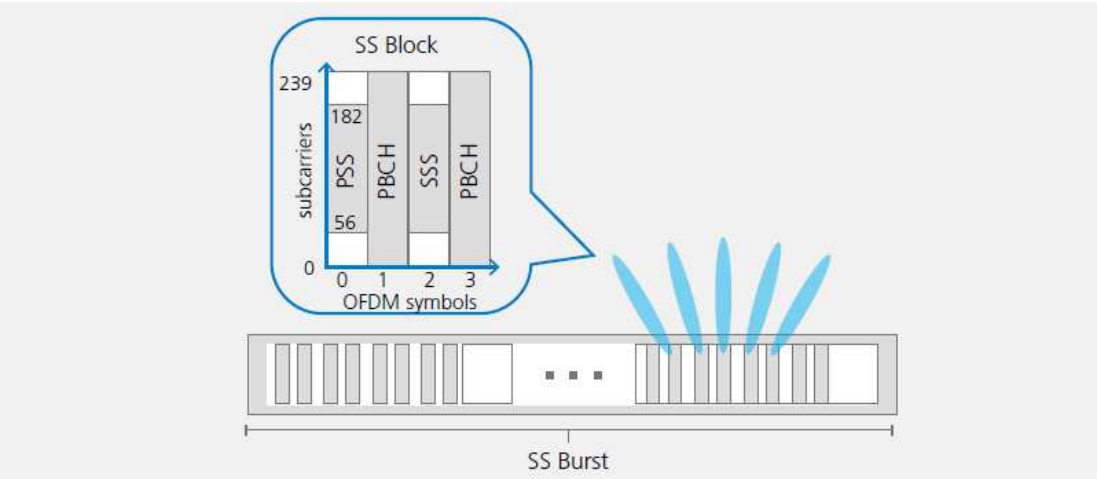

Figure 3.9: Directional SS blocks transmission[29]

After the beam sweeping operation, the UE device evaluates and selects the beam with the maximum SNR through the beam measurement and beam determination operations. The last procedure, i.e., beam reporting, can occur in two different ways: Non-Standalone mode (NSA), which considers both the downlink (DL) and the uplink (UL) case, and the Standalone mode (SA).

In NSA-DL mode, thanks to the control plane integration with the LTE overlay, the UE uses the LTE connection to report the optimal set of directions to the gNB. In this way, to perform the beam reporting or the IA procedure, the user does not need to wait for an additional beam sweep from the gNB [8]. The gNB then schedules an immediate random access opportunity (to determine the first available resource which can be used by UE to transmit without colliding with other devices) for the determined direction with the full beamforming gain [29]. Moreover, the LTE link can be used also in the case of a link failure, consequently there is a data-plane fallback to the sub-6-GHz connection, while the user recovers the mmWave link. In Fig.3.10 mode are shown signal and messages exchanged during the NSA-DL beam management procedure with the beam, reporting step of the

IA.

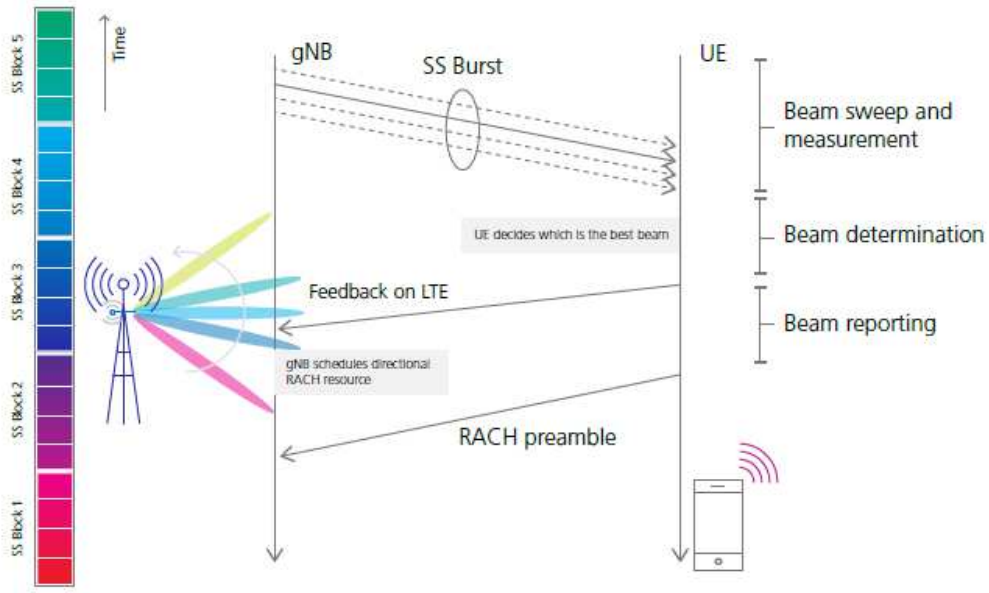

Figure 3.10: IA in NSA-DL mode. [29]

In contrast to LTE schemes, the NSA-UL model is based on the channel quality of the UL rather than the DL signals. In this model, the UE searches for synchronization signals from 4G cells, involving a fast detection since it can be performed omnidirectionally. In the NSA-UL procedure, shown in Fig.3.11, each UE broadcasts SRS (i.e., Sounding Reference Signal. that is signals used to monitor the UL channel quality, transmitted by the UE and received by the gNBs) changing the directions in time. The gNB scans all its angular directions monitoring the strength of the received SRSs. Based on that, each mmWave cell of the considered gNB sends this information to the eNB (i.e., the 3GPP-compliant implementation of 4G LTE BS) which, through the signal quality information gathered by the gNB-UE pair communication, can receive the complete directional knowledge over the cell it controls and provide the maximum performance matching the beams of the transmitter and the receiver. [8]. At this point the coordinator reports to the UE the gNB which provides the best performance and the optimal direction, therefore it notifies also the

selected gNB the optimal direction in order to steer the beam to serve the UE.

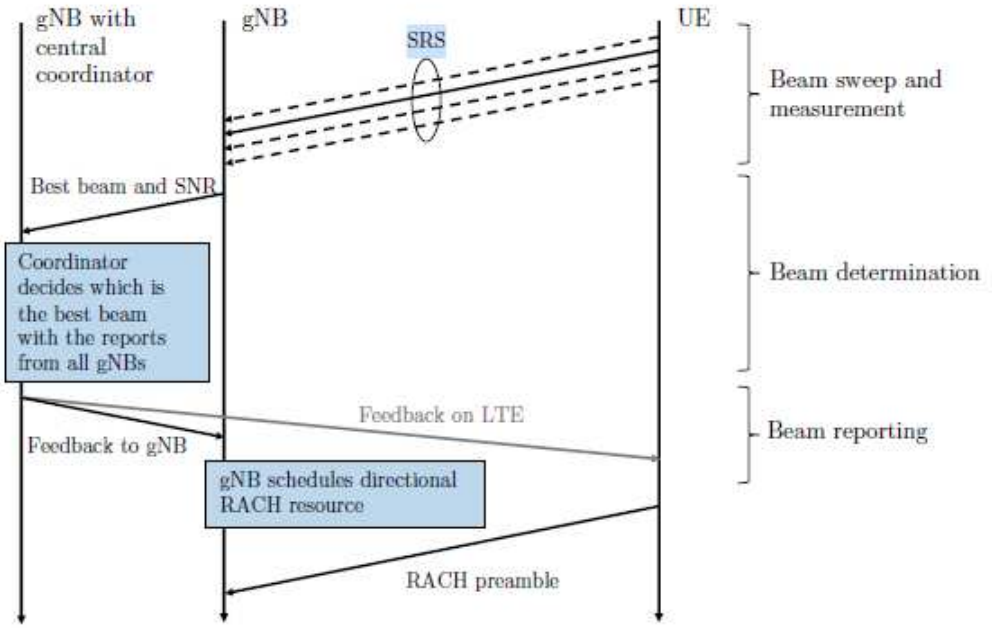

Figure 3.11: IA in NSA-UL mode. [8]

The SA-DL mode is not based on an LTE connection, and the user waits for its gNB to schedule a random access channel (RACH) opportunity toward the best direction that the UE just determined, which in the worst case may take a number of RACH opportunities equal to the number of directions to investigate. This step allows to perform random access and inform the selected serving infrastructure of the optimal direction through which to steer the beam in order to be properly aligned. Then, the gNB specifies for each SS block one or more RACH opportunities with a certain time and frequency offset and direction. This allows the user to know when to transmit its RACH preamble toward the direction as determined by the gNB [35] [36]. The beam reporting process for SA-DL mode can require an additional complete directional scan of the gNB for SS block transmission, therefore the time to access the network increases. Fig.3.12 represents the SA-DL beam management procedure, where is visible

the different duration of the three phases since it depends on the actual configuration of the network parameters.

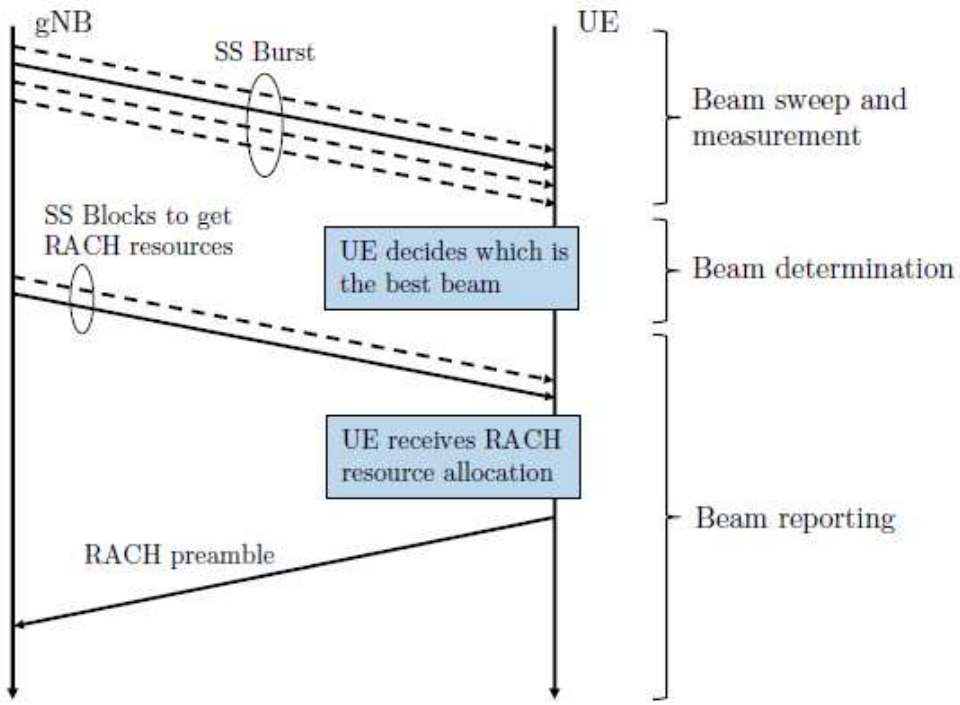

Figure 3.12: IA in SA-DL mode. [8]

3.5.2 Connected mode beam management

The goal of beam management in connected mode is to maintain the alignment of the transmitter and receiver beams when the user is moving. This operation is known as beam tracking and uses downlink CSI-RS (Channel State Information Reference Signal).

CSI-RSs measure and report channel conditions through the Channel State Information and can be used for Radio Resource Management (RRM) measurements for mobility management purposes in connected mode [8]. It is possible to combine multiple CSI-RS to the same SS burst in order to obtain synchronization [37] [38], and

then use that as a reference to search for CSI-RS resources with specified frequency and time offsets.

In the CSI-RS window configuration are set the periodicity and time/frequency offset relative to the associated SS burst. In [8] are presented two options for the time offset of the CSI-RS transmissions, which are represented in Fig.3.13 and Fig.3.14.

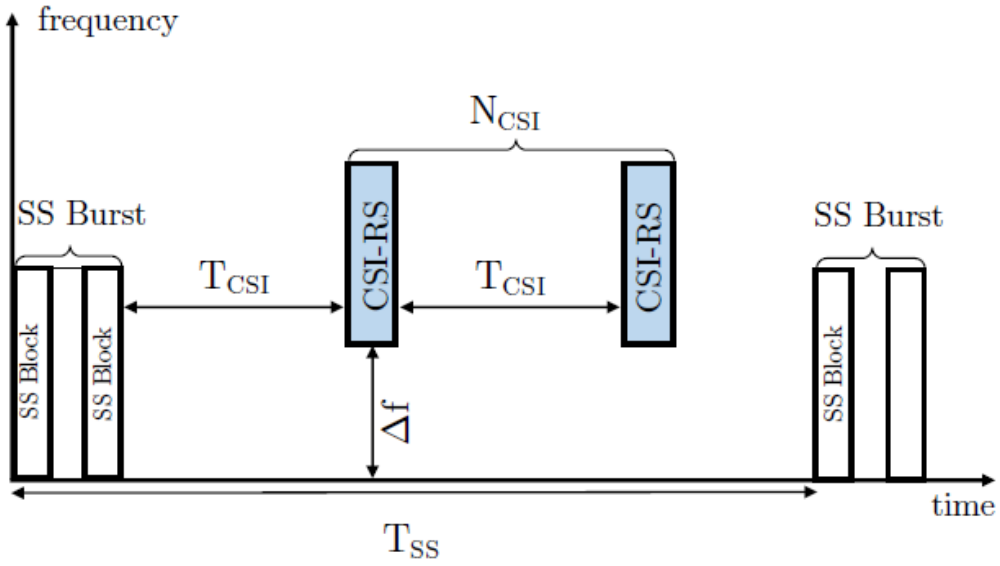

Figure 3.13: First CSI-RS is sent T_{csi} ms after an SS burst. [8]

In the first case, the transmission of the first CSI-RS is scheduled T_{csi} ms after the end of an SS burst, while the second one provides an additional parameter called O_{csi} which represents the time interval between the end of an SS burst and the first CSI-RS. As described in [39], the periodicities for the CSI-RS transmissions are $T_{csislot} \in$ [5,10,20,40,80,160,320,640] slots, therefore the periodicity in time depends on the slot duration. Considering the need to periodically identify the best directions for the beams of the transceiver to maintain the alignment between the communication nodes, i.e., beam search operation, both the SS and the CSI-RS-based results can be jointly used to consider the different coverage achieved with different beamforming configurations. Since CSI-RS are transmitted on a wide

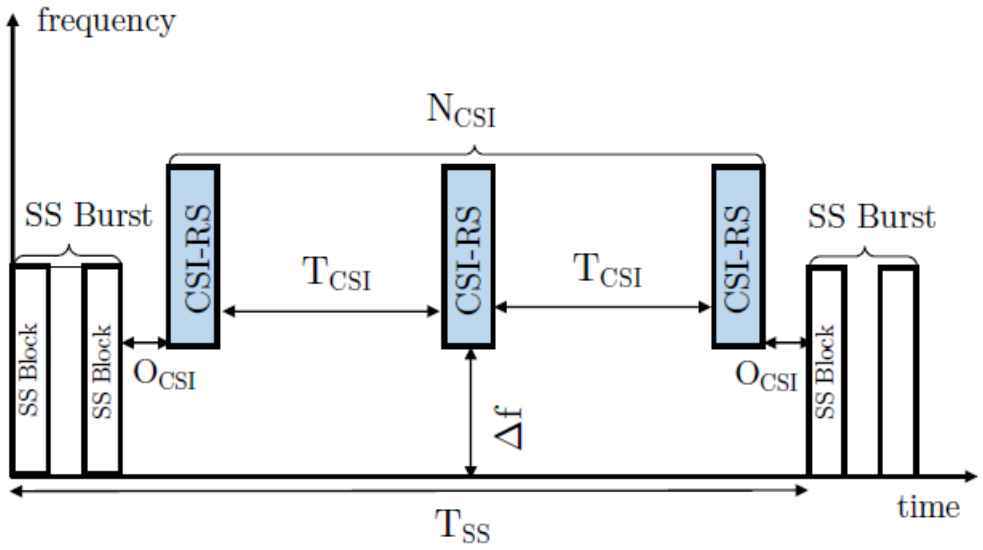

Figure 3.14: First CSI-RC is sent O_{csi} ms after an SS burst. [8]

spatial domain coverage with a huge number of narrow beams, this may incur into overhead and power consumption problems [40]. This explains the use of a subset of those beams, based on the locations of the active UEs. For example, as explained in [8], the measurements results referring to a subset of a transmitting directions and based on SS blocks, can increase the energy efficiency by narrowing down the CSI-RS resource sets based on which a user performs measurements for beam management.

Chapter 4

The ns-3 Simulator

4.1 Introduction

The ns-3 simulator is a discrete event simulator targeted primarily for research and educational use, which develops an open source simulation environment focused on networking research. It is based on the contribution of a community of people that continuously improves the project and allows the realization and simulation of several standard networks and protocols.

At this stage, the research community has released two ns-3 modules to simulate 5G networks, namely 5G-LENA (developed by CTTC) and ns3-mmwave (developed by the University of Padova)[41], which are largely considered amongst the most accurate tools to simulate 5G networks. The ns-3 mmWave module is designed to be a fully customizable model where the user can plug in 5G-NR compatible carrier parameters such as frequency, bandwidth, frame structure, explaining the behavior of millimeter wave channel and devices. The flexible use of this module allows the researchers to model different scenarios without altering the source code.

4.2 The ns3-mmWave module

The first version of mmWave module was released in May 2015 and it is developed by NYU, in collaboration with the University of Padova. The module has undergone several updates, and now incorporates different features in separate branches, like D2D, LAA, LTE-U, IAB, NR V2X, and a ray tracing implementation, which permits accurate simulations in the context of 5G.

The ns-3 simulator is organized into multiple folders. The *src* folder provides a collection of C++ classes, which implement a wide range of modular simulation models and network protocols.

Different network scenarios can be simulated aggregating the modules and making ns-3 especially useful for cross-layer design and analysis. Each module is organized in multiple subfolders with the documentation and the source code of the model itself, the helpers, which hide to the final user the complexity involved in building a complete scenario, the examples, and the test. Finally, in scratch folder are placed the temporary scenarios that can be test on-going. Besides the basic structure, there are other modules for networking protocols, wireless protocols, mobility, and data collection [41].

The module, whose architecture is depicted in Fig.4.1, allows to simulate an end to end simulations of 3GPP cellular networks. It is based on the fully customizable time division duplex (TDD) frame structure, a radio characterization that includes MIMO techniques such as beamforming, an ad-hoc error model which abstracts the decoding process at the receiver and an interference model.

The next sections describe more in depth the features and the details of the 3GPP implementation on the ns3-mmwave module.

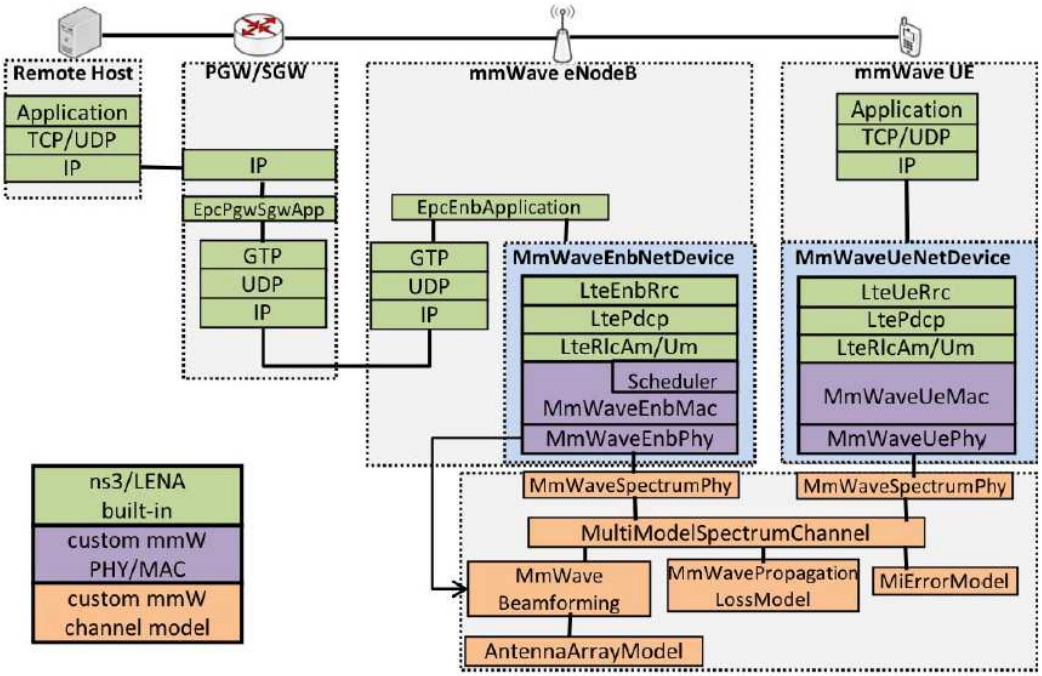

Figure 4.1: Class diagram of the end-to-end mmWave module.[41]

4.2.1 PHY layer

4.2.1.1 Frame structure

This section describes the key features of the mmWave PHY layer. Specifically it is implemented a TDD frame and subframe structure which has similarities to TDD-LTE, but allows for more flexible allocation of control and data channels within the subframe, since they are designed to be configurable and support short slots to evaluate different potential designs and numerologies [41]. This choice allows to improve the use of wider bandwidths and take advantage of channel reciprocity for channel estimation. In addition, the TDD structure reduces the latency of radio links [42] [43]. Based on the previous considerations, ns-3 mmWave module implements a TDD frame structure, in order to evaluate different potential designs and numerologies.

Fig.4.2 shows the parameters for configuring the mmWave PHY layer and accessible through the attributes of MmWavePhyMacCommon class, which stores all the configuration parameters used by the

PHY and MAC classes. In a mmWavePhyMacCommon object the duration of one slot is represented by Transmission Time Interval (TTI) and is implemented by the function mmWavePhyMacCommon::GetTTI(), while bandwidth is set by the function GetSystemBandwidth().

Parameter Name	Default Value	Description
SubframePerFrame	10	Number of subframes in one frame
SubframeLength	100	Length of one subframe in μs
SymbolsPerSubframe	24	Number of OFDM symbols per slot
SymbolLength	4.16	Length of one OFDM symbol in μs
NumSubbands	72	Number of subbands
SubbandWidth	13.89	Width of one subband in MHz
SubcarriersPerSubband	48	Number of subcarriers in each subband
CenterFreq	[6-100]	Possible carrier frequencies in GHz*
NumRefScPerSymbol	864 (25% total)	Reference subcarriers per symbol
NumDlCtrlSymbols	1	Downlink control symbols per subframe
NumUlCtrlSymbols	1	Uplink control symbols per subframe
GuardPeriod	4.16	Guard period for UL-to-DL mode switching in μs
MacPhyDataLatency	2	Subframes between MAC scheduling request and scheduled subframe
PhyMacDataLatency	2	Subframes between TB reception at PHY and delivery to MAC
NumHarqProcesses	20	Number of HARQ processes for both DL and UL

*The NYU channel model [32] supports only 28 and 73 GHz.

Figure 4.2: Parameters for configuring the mmWave PHY layer.[41]

The frame and subframe structures, inside which a variable number of symbols can be assigned by the MAC scheduler and designated for either control or data channel transmission, are already described in Chapter 2.

Physical layers of the BS and UE can be modeled with mmWaveEnbPhy and mmWaveUePhy classes respectively. The transmission and reception of physical control and data channels are controlled by the physical layer, which delivers data packets and control messages to the MAC layer. Physical layer is responsable also for simulating the start and the end of frames, subframes and slots.

Based on the user-specified subframe length, the start and the end of each subframe are scheduled at fixed periods, and are handled by MmWaveEnbPhy and MmWaveUePhy classes through the call to StartSubFrame() and EndSubFrame(). The MAC dynamically configures the timing of variable TTI slots, which are controlled

by scheduling the StartSlot() and EndSlot() functions. In particular, to configure the TTI timing, is called the SetSfAllocInfo() function, which contains all the information about the element allocation for some future subframe index specified by the MAC, and is described in MAC-PHY SAP. At the beginning of each subframe the MAC layer, after receiving a subframe indication, triggers the scheduler to allocate a future subframe. After reception of DCI messages, the UE PHY inserts the allocation information on SfAllocInfo objects, which in turn, specify contiguous ranges of OFDM symbol indices occupied by a given slot. SfAllocInfo objects include also some symbol's attributes, such as *DL* or *UL*, and *control* (CTRL) or *data* (DATA). Once data packets and the control messages are generated by MAC, they are mapped to a specific subframe and slot index in the *packet burst map* and *control* message map, respectively.

The eNB PHY starts the transmission of a data slot by calling the AntennaArrayModel::ChangeBeamformingVector() function, thereby the transmit and receive beamforming vectors are updated for both the eNB and the UE. Considering the control slots, since it is assumed an ideal control channel, there is not any beamforming update. To transmit data or control slots, are called StartTxDataFrame() and StartTxCtrlFrame() function respectively, which belong to MmWaveSpectrumPhy class. When data packets are received, PHY layer computes the SINR of the received signal considering the pathloss, MIMO beamforming gains and frequency-selective fading. This operation implies the generation of Channel Quality Information (CQI) report, which represents a feedback to the BS by UL data or control slots.

The PHY layer also incorporates the error model, which is a probabilistic approach that allows the receiver to drop some packets based on the SINR, and deliver, by the MmWavePhy instance, to the MAC layer SAP only the correct ones.

4.2.1.2 Channel model

In order to provide a trade-off between computational complexity, flexibility and accuracy of the results, the ns-3 mmWave module allows the user to choose among three different channel models.

The most flexible and detailed is the *3GPP Statistical Channel Model*, which is described in [44]. In this model is considered the frequency spectrum above 6 GHz (i.e. 6-100 GHz band) and it provides also several features that can be plugged into the basic model, in order to simulate, for example, spatial consistency and random blockage. The 3GPP model implements different scenarios, as urban environment, rural, and indoor. This model defines the pathloss in MmWave3gppPropagationLossModel class, providing a statistical LOS/NLOS condition characterization and a pathloss computation based on indoor and outdoor penetration loss. The LOS condition is determined by MmWave3gppBuilding PropagationLossModel class, according to the position of the UE and gNB, and the presence of obstacles in the scenario.

The small-scale fading model, which is very detailed and computationally demanding, is implemented in the MmWave3gppChannel class. The channel is described by a channel matrix $H(t,f)$, where t represents the time and f is the frequency. The dimension of the matrix are UxS, where U and S are the number of antennas at the receiver and the transmitter respectively [41]. Each entry of the matrix depends on different multipath components, called clusters, which have different delays and received powers. The channel matrix is generated by a method of MmWave3gppChannel class, which stores the coefficient for each transmit element s, received element u, and cluster n, that can be retrieved by other methods to update the channel matrix and compute the beamforming gain. As mentioned before, the *3GPP Statistical Channel Model* can be used also to account for

spatial consistency of mobility-based simulations. In fact, for simulations in which the mobility is an important factor, the spatial consistency of the channel can be simulated by enabling this option in the MmWave3gppChannel class. This class implements also the blockage optional feature, that can be used to represent the attenuation caused by human body or by external elements such as trees or cars. In particular, the model described in [41] can only distinguishes between self-blocking and non-self-blocking, as described in Fig.4.3. The model generates K + 1 blocking regions, one for self-blocking, K for non-self-blocking. The attenuation is different for the two cases, based on the scenario and on the angles of arrival for non-self-blocking, fixed at 30 dB for self-blocking case. If both the spatial consistency and the blockage are used, the channel with both features is synchronized. This means that the cluster blockage is update before the channel coefficients are recomputed with spatial consistency procedure [41].

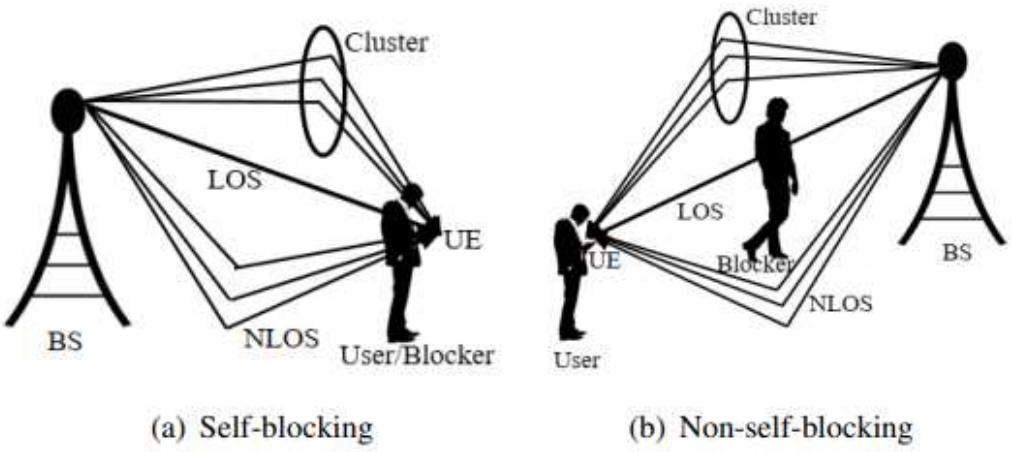

Figure 4.3: Blocking scenario [45]

The second channel model provided by ns-3 mmWave module, i.e. *Ray-Tracing or Measurement Trace Model*, is based on traces from measurements or third party ray-tracing software. This represents a realistic channel model, but the simulations are limited to specific ray-tracing routes, since the trace samples need to contain the number

of paths and the propagation loss, delay, angle of arrival and angle of departure for each path. Any ray-tracing software, whose input is represented by the simulation scenario, can be used to generate the channel information.

The third model is the *NYU Statistical Model*, implemented in [46]. It provides two channel models that capture the LOS/NLOS condition differently. The first is based on the a statistical characterization of the LOS state, while the second uses the ns-3 building modules to discover obstacles between the UE and the eNB. If the virtual line which connects the UE and eNB intersects any object, the state is NLOS, otherwise is LOS.

This model is based on MATLAB traces and available only for the 28 and 73 GHz frequencies. Since the channel matrices and optimal beamforming vectors do not depend on the distance between the UE and the eNB, channel matrices and optimal beamforming vectors are pre-generated in MATLAB to reduce the computational complexity in ns-3. In particular, at the beginning of each simulation are loaded 100 instances of the spatial signature matrices and beamforming vectors. Furthermore, to simulate realistic channel with large-scale fading, the channel matrices are periodically updated. This information is specified by the LongTermUpdatePeriod attribute of the MmWaveBeamforming class. The small-scale fading instead, is calculated at every transmission, by which is obtained the speed of the user directly from the mobility model. Other environment's parameters are assumed constant over the entire simulation time. Fig.4.4 shows an example of average SINR plots for the three channel models.

4.2.1.3 Beamforming

If long-term statistical channel models are considered, the beamforming vectors are directly loaded from MATLAB generated files, while for the other channel models are implemented the *long-term covari-*

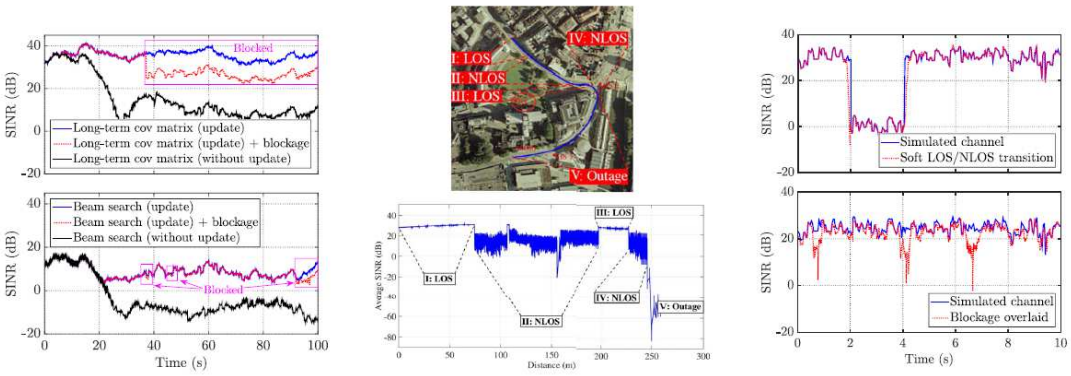

(a) 3GPP statistical channel model (b) Ray-tracing Trace Model (c) NYU Statistical Model

Figure 4.4: Example of average SINR plots for the three channel models [41]

ance matrix method and *the beam search method*, which compute the beamforming vectors. The beamforming architecture which is provided is analog.

Considering the *long-term covariance matrix method*, the transmitter computes the spatial correlation matrix $\mathbf{Q}_{tx} = \mathbb{E}[H(t,f)\mathbf{H}(t,f)]$, where the expectation is taken over the frequencies and some interval of time. The analog operation, i.e. $\mathbf{Q}_{rx} = \mathbb{E}[H(t,f)\mathbf{H}(t,f)]$, is done for the receiver. The spatial covariance matrix is estimated by the transmitter and the receiver from synchronization signal and beam scanning. Consequently beamforming vectors can be computed from the maximal eigenvectors of the covariance matrix [47].

4.2.1.4 Interference

The strong directionality propagation due to a high dimensional phased array does not remove the problem of interference. In fact, this problem is still present and it is not easy to solve in simulations.

The results in [48], depicted in Fig.4.5 show that the majority of the links are still interference-limited for some dense topologies. Moreover, considering the intra-cell interference (i.e. from devices of the same cell) which can be neglected both in TDMA and FDMA operation, it needs to be explicitly computed in the case of Spatial

Division Multiple Access (SDMA)/Multi-User MIMO, where users are multiplexed in the spatial dimension but operate in the same time-frequency resources [41]. This is the reason why in [41] is proposed an interference scheme in which are considered the beamforming vectors associated with each link.

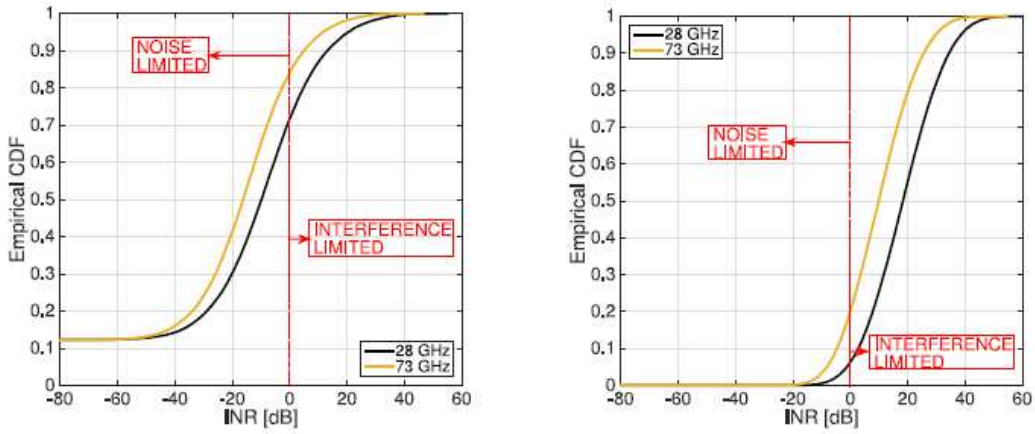

(a) Empirical CDF of the INR for $\lambda_{UE} = 300$ UEs/km^2 and $\lambda_{eNB} = 30$ BSs/km^2.

(b) Empirical CDF of the INR for $\lambda_{UE} = 1200$ UEs/km^2 and $\lambda_{eNB} = 120$ BSs/km^2.

Figure 4.5: INR trends at different user and BS density levels [41]

The SINR between BS_1 and UE_1 is computed knowing the channel gain of both the desired and interfering signal, i.e.,

$$G_{11} = |\mathbf{w}^*_{rx_{11}} H(t,f)_{11} \mathbf{w}_{tx_{11}}|^2 \tag{4.1}$$

$$G_{21} = |\mathbf{w}^*_{rx_{11}} H(t,f)_{21} \mathbf{w}_{tx_{22}}|^2 \tag{4.2}$$

where $\mathbf{w}_{rx_{i,j}}$ represents the beamforming vector of receiver i and transmitter j, while $\mathbf{w}_{tx_{i,j}}$ is the beamforming vector of receiver j and transmitter i.

After the computation of channel gains, the SINR can be obtained

as in the following equation:

$$SINR_{11} = \frac{\frac{P_{Tx11}}{PL_{11}}G_{11}}{\frac{P_{Tx22}}{PL_{21}}G_{21}+BW\times N_0} \tag{4.3}$$

where P_{Txii} represents the power of transmission, PL_{ij} represents the pathloss between the BS and the user, and finally $BW \times N_0$ is the thermal noise.

4.2.2 MAC layer

Considering the dependence on analog beamforming, TDMA is assumed to be the most appropriate scheme for mmWave access. Different designs have been TDMA-based[49] [50] [51], while others consider also SDMA for the control channel [42]. SDMA or FDMA can be used only for digital beamforming, since in this case the BS would transmit or receive in multiple directions at the same time.

One of the most important innovation for 5G MAC layer is latency. In fact, the Key Performance Indicator of 1 ms over-the-air latency has been proposed as a 5G requirements by ITU. However, considering the use of fixed slot lengths, the resource utilization becomes really poor, especially in scenarios where many devices need to transmit/receive. Consequently variable TTI-based TDMA frame structures and MAC schemes have been proposed in order to make more flexible the transmissions, since slot sizes can vary according to the length of the packet.

The MAC layer is implemented by the class MmWaveMac, which is the base class for the MmWaveEnbMac for the eNodeB, and the MmWaveUeMac for the user. This layer is the link between the upper layers and the physical one and delivers data packets coming from the upper layers to the physical layer and viceversa. In addition, it communicates to the PHY layer the scheduling and the resource

allocation.

The MAC-SCHED service access point (SAP) connects the eNodeB MAC layer and the scheduler, as depicted in Fig.4.6, MAC and scheduler modules, while MAC and PHY layers are connected through the PHY SAP interface.

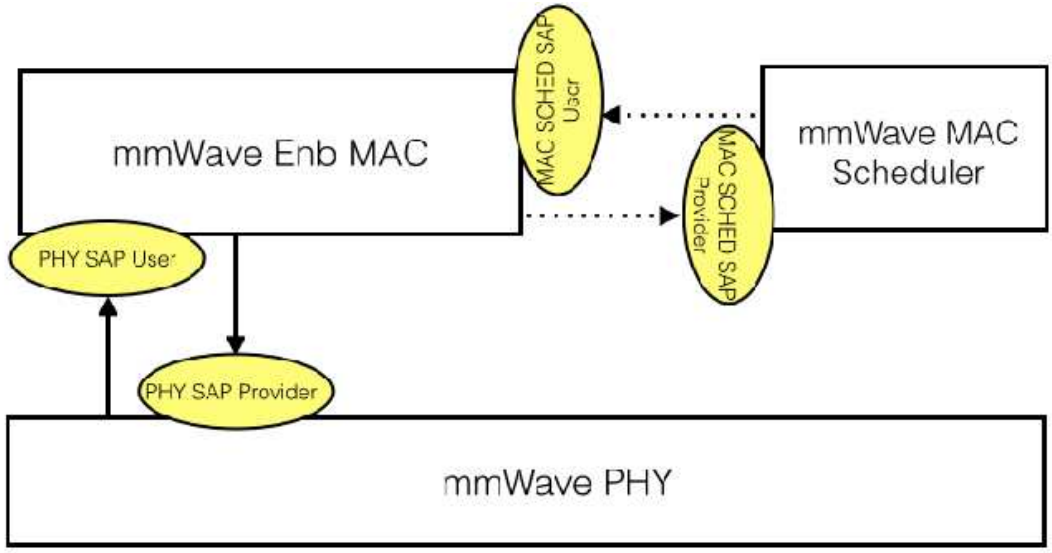

Figure 4.6: PHY, MAC and scheduler modules [46]

4.2.2.1 Adaptive Modulation and Coding

The Adaptive Modulation and Coding (AMC) is a mechanism used to compute the most appropriate modulation and coding scheme for the transmission, and it is measured using CQIs. This can be translated into mapping the CQI into the Modulation and Coding Scheme (MCS), and computing the available TB size for a subframe given the MCS. The MmWaveAmc class, which implements the AMC, is based on LENA module, even though some additional methods were necessary to support the dynamic TDMA MAC scheme and the frame structure.

4.2.2.2 Scheduler

This section presents four scheduler classes based on TTI scheme, which differ significantly from the OFDMA-based schedulers available in ns-3 LENA. This is a consequence of the time-domain allocation of the symbols within a periodic subframe to different users in the DL or UL direction. The procedure for estimating the optimal MCS and determining the minimum number of symbols required to schedule the data in the user's Radio Link Control (RLC) buffers is common to each of the schedulers described in the following.

The *Round Robin (RR) Scheduler* is implemented by the MmWaveFlexTtiMacScheduler class and supports the TTI scheme previously described. This scheduler assigns OFDM symbols to user flows in Round Robin order. To realize that, first the total number of users with active flows are calculated, then the total available data symbols in the subframe are divided evenly among users. If the user requires a lower number of symbols to transmit its entire buffer, the remaining symbols are distributed among the users with active flows.

The *Proportional Fair (PF) Scheduler*, provided by MmWaveFlexTtiPfMacScheduler class, prioritizes traffic for high SINR users maintaining some measure of fairness by ensuring that low SINR.

The *Earliest Deadline First (EDF) Scheduler* is implemented by the MmWaveFlexTtiEdfMacScheduler class, and provide a queue based policy that weights flows by their relative deadlines for packet delivery.

The *Maximum Rate (MR) Scheduler*, described by MmWaveFlexTtiMrMacScheduler class, schedules only the users with the highest SINRs to maximize cell throughput. The MR scheduler can suffer from extremely poor fairness when there are both high rate and low rate users, and some users may not be scheduled at all, therefore it becomes impractical for any real-world multi-user system, even though

can still be useful for testing performance.

4.2.2.3 PHY-MAC

The processes that describe the communication steps between the MAC and the PHY using the MAC-PHY SAP interface are the following[46]:

- The subframe indication is sent at the beginning of each slot and in the case of slot 1 for a specific subframe represents the trigger for the scheduling procedure. The subframe indication is sent by the PHY layer to the MAC;
- The eNodeB can be connected with multiple UE maintaining data queues for each of them. The MAC layer sends to the PHY layer the scheduled number of packets which depends on the allocated resources and the scheduling scheme;
- After receiving the scheduling and resource allocation from the scheduler, eNodeB MAC forwards this information to PHY through the mmWaveResourceAllocation message. Then the PHY layer of the BS sends this message to all the users that are connected with it;
- The PHY layer of the user computes the CQI relying on the received data slots SINR, and sends it to the BS in the next uplink transmission. Once the eNodeB has received the information on the CQI, relays it to the MAC.

4.2.2.4 MAC-SCHED

The processes that characterize eNodeB MAC are the following[46]:

- When it receives information on slot 1 of a specific subframe, MAC sends to the scheduler a trigger request. In reply to the trigger, the scheduler returns a decision which is communicated in the Scheduling Configuration Indication;

- As mentioned before, eNodeB MAC receives the CQI information from the PHY and sends it to the scheduler. This information is crucial for the next decision on schedule.

4.3 NS-3 simulations

Since in the current version of the ns-3 mmwave the beamforming vectors are determined according to codebook-based approach, the 5G NR standard requirements, which implement a cell-search algorithm based on SS blocks, are not satisfied. This thesis aims at solving this problem by implementing the beam management procedure. To realize that, the first step was to introduce the SS block signal, by making changes in the MmWaveEnbMac class. According to [8], slot's symbols are marked as occupied if meet specific requirements, that are related to the position within the slot, the number of the SS block in a burst, the periodicity of the burst, and if the SS block is allocated into the first 5 ms of an SS burst. After this operation, SS blocks were scheduled by modifying the DoSchedTrigger() function of MmWaveFlexTtiMacScheduler class. After the scheduling operations, the focus was moved on physical layer's implementation, where was created an ad-hoc function called ConfigureBeamforminForSsb() in the MmWaveCodebookBeamforming class. This function initializes a matrix, whose dimensions are U x S, where U is the number of beams handled by the BS, and S is the number of beams handled bu the user. This variable is based on the number of antenna elements, as explained in [8]. This matrix is then filled with the values of the SINR estimated for each couple of beam. Once the matrix is complete, the index of the codebooks that generate the highest SINR is saved. The final step was the update of the ConfigureBeamforming() function in MmWaveSpectrumPhy class. Within this function are set, based on the characteristics of the analyzed symbol, the beamforming

procedure to perform: if the symbol was scheduled as SS block, the subsequent beamforming function is ConfigureBeamformingForSsb(), otherwise the following step is represented by SetBeamformingVectorForDevice. Once all the functions are implemented and functional, the simulation script is implemented.

In order to perform ns-3 simulations, the following steps are performed:

- beamforming model is selected;
- transmitter and reveiver node containers are created to represent the UE and the BS;
- channel model is configured;
- SS block parameters are selected;
- power and noise parameters are set;
- UE antennas and BS antennas are configured;
- remoteHost is initialized;
- Internet is configured;
- transmitter and receiver devices are created;
- server and client application are initialized and activated, therefore data can be transmitted during the simulation;
- Simulator::Run starts the simulation, while the simulation duration is set by the command Simulator::Stop.

In next chapter are summarized all the parameters set in the simulation to perform a system-level analysis of beam management protocol under different scenarios.

Chapter 5

Simulations and performance evaluation

5.1 Simulated scenarios and parameters

The performance evaluation has been carried out using the ns-3 mmwave framework. The simulated scenario is configured as follows:

- the deployment is not static, we assume the UE is moving during the simulation;
- we assume an indoor scenario, i.e., a room;
- channel model is addressed by Ray Tracers, which is used to describe reliable channel, based on a deep understanding of the propagation characteristics of the mmWave signal, and described in [52];
- the work is based on analog beamforming, thus devices can transmit or receive one signal at a time.

The parameters in the simulated scenario mimic the communication between a 5G NR UE and an indoor BS. The UE speed is taken in accordance with [52], with the goal of reusing the same channel traces [52]. An exhaustive list of the simulation parameters is reported in Table 5.1.

Parameter	Value
OFDM symbols per slot	14
OFDM symbol duration	17.857 μs
TX power	24
Noise Figure	12
UE speed	1.2 m/s
Beamforming model	Analog
Propagation conditions	LoS, NLoS
Simulation time	15
N_{SS}	16, 32, 64
T_{SS}	40, 80, 160
Number antenna elements	4, 16, 64

Table 5.1: Simulation parameters.

Accordingly, we consider the L-shaped hallway scenario presented in [52], and set the UE speed to 1.2 m/s, as depicted in Fig.5.1.

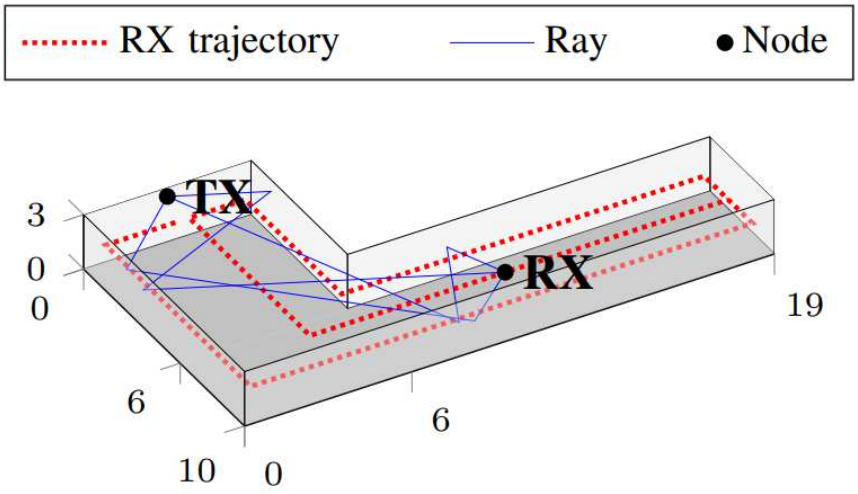

Figure 5.1: Visual representations of the proposed L-room scenario. Distance measured in meters, taken from[52]

First, we present results concerning the PHY layer performance of the system, measured in terms of SNR. Then, we focus on the system-level performance, inspecting throughput, latency and packet drop rate.

5.2 Results

5.2.1 PHY layer performance

We begin our analysis by studying the impact of the number of antenna elements at the gNB on the end-to-end SNR. In general, the antenna elements can be deployed as uniform linear (ULA) or planar arrays (UPA), and the latter can be arranged as either rectangular or square arrays. We follow the reasoning of [8], and consider UPAs and ULAs for gNB and UE respectively. The number of antenna elements at the UE is 2, which remains fixed for all the simulations, while the set of possible numbers of antenna elements for the gNB is $\{4, 16, 64\}$. The parameters considered to analyze this case are the number of SS blocks per burst N_{SS}, and the burst period T_{SS}. In order to limit the number of considered SNR samples, with the goal of improving the plots' readability, the frequency sampling is reduced from 1.1 kHz to 52.5 Hz.

In principle, the SNR is mainly impacted by:

- the distance between the UE and gNB, since long distances lead to higher pathloss;
- the channel condition, since during the simulation it evolves from a condition to another;
- the specific position of the UE. In fact, as it changes over time, the optimal beam also varies. However, since the beams are not reestimated at every transmission, for a period of time the beams are possibly sub-optimal.

These considerations are useful to interpret the following graphs. In the first example N_{SS} is set to 16, therefore we consider a low number of SS blocks per burst, while T_{SS} is set to 160 ms, the longest burst period treated in this thesis. The result is depicted in Fig.5.2.

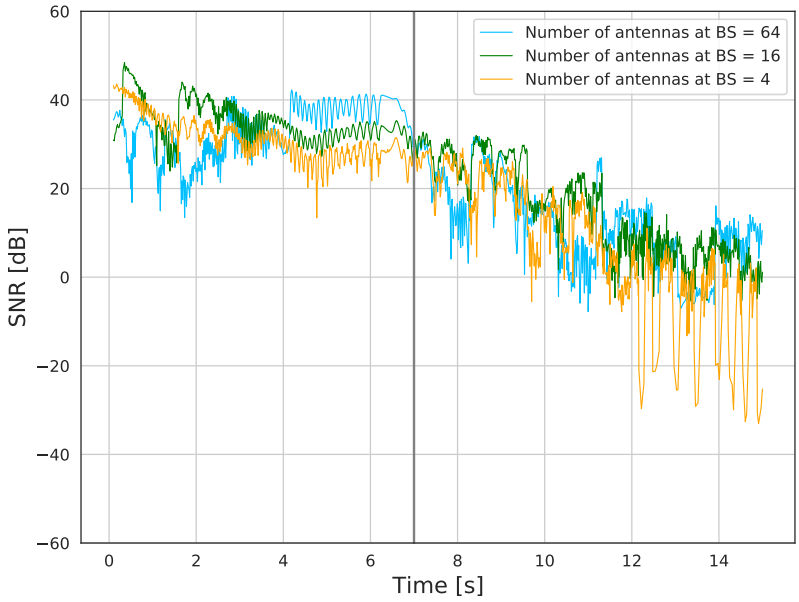

Figure 5.2: SNR vs time for $N_{SS} = 16$, $T_{SS} = 160$ ms. The black vertical line represents the time instant during which the UE ends up in a NLoS condition.

It is possible to distinguish essentially two phases during the simulation: in the first phase the UE is in a LoS condition, while in the second it is in NLoS condition. Different SNRs for a specific gNB antenna configuration are caused by the alignment of the beams. Moreover, the difference in the SNR is also given by the different gain due to the fact that with more antennas it is possible to produce narrower beams. Considering the long burst period, and the small value of N_{SS}, the beams require large period to be aligned, in particular the BS with 64 antenna elements, which is aligned for the first time after 1.28 s. In the time intervals during which the gNB and the UE are aligned with each other, the highest SNR values are reached by the antenna configuration featuring the highest number of radiating elements, move after aligned with each other, then the UE enters a NLoS condition. At this point is clear that the SNR evolves consistently with the mobility of the UE: the SNR suddenly degrades when the UE enters a NLoS condition, while is maximized when it is in LoS

with its serving BS.

As explained in Sec.3.2, the number of antenna elements dictates both the directionality and the beamfroming gain, as depicted in Fig.5.3. This correlation explains why in some cases, for instance in the interval 7.5-8.5 s, 10.5-11.5 s, the SNR obtained with the biggest antenna array is slightly lower compared to other antenna configurations, since if the BS is not aligned with the UE, the beamforming gain is significantly reduced, while the beamforming gain of a BS with less antenna elements has a more linear behaviour.

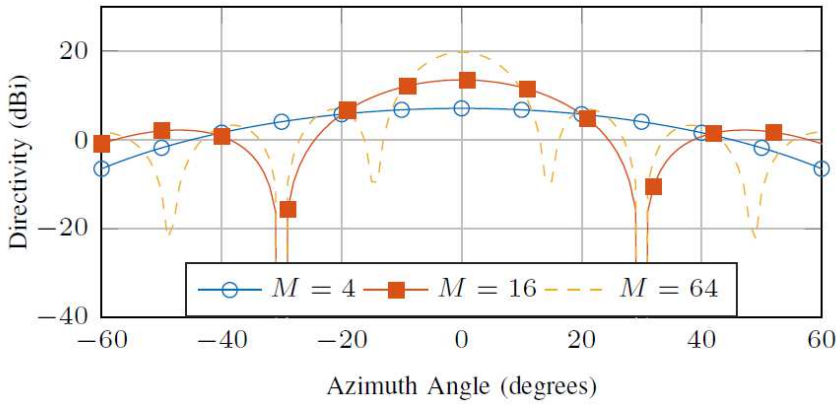

Figure 5.3: Relationship between beamwidth and antenna array size. Taken from [8]

Then, we consider a more aggressive beam management configuration by fixing $N_{SS} = 32$ and $T_{SS} = 80$ ms. With these parameters the configurations with large number of antenna elements can reach higher gains. In fact, comparing the results depicted in Fig.5.4, and the ones reported in Fig.5.2, the SNR is clearly higher than the previous example, considering that for both the 32 and 64 gNB antenna configurations it exceeds 50 dB.

After 7 s, the UE enters a NLoS condition, thus exhibiting a degradation of the SNR. In this case, differently from the previous, in NLoS condition the SNR achieved by the BS with more antenna elements is still a bit higher, i.e. 5 dB, than the ones generated by BS with 16

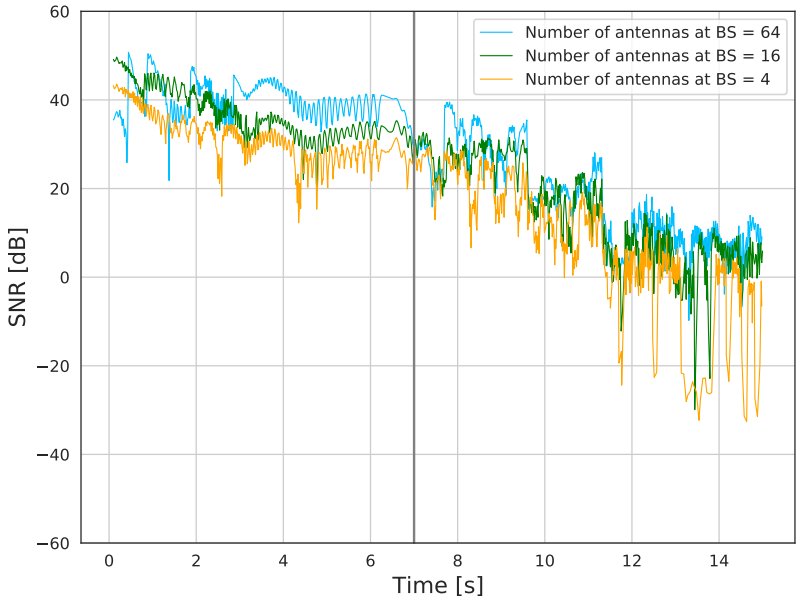

Figure 5.4: SNR vs time for $N_{SS} = 32$, $T_{SS} = 80$. The black vertical line represents the time instant during which the UE ends up in a NLoS condition.

and 4 antennas.

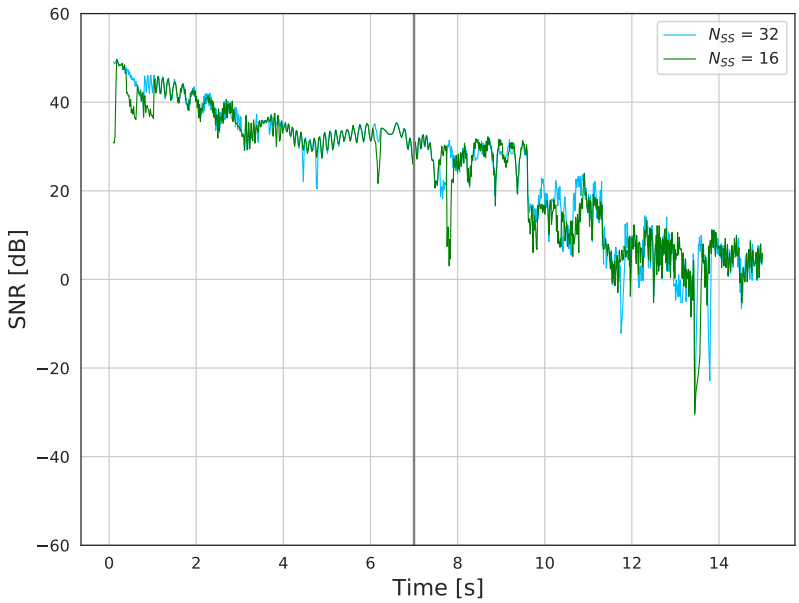

Figure 5.5: SNR vs time for number of antennas at BS = 16, $T_{SS} = 80$, $N_{SS} = \{32,16\}$. The black vertical line represents the time instant during which the UE ends up in a NLoS condition.

After the comparison between different antenna configurations, this parameter is kept fixed and the results are analyzed changing N_{SS} and T_{SS}. First, we consider 16 antenna elements at the gNB, $T_{SS} = 80$ ms and $N_{SS} = \{16,32\}$. As can be seen in Fig.5.5, both the considered values of N_{SS} lead to similar PHY layer performance. The outcome shows a really similar behaviour for both the models. This proves that, considering a 16 element antenna array, and $T_{SS} = 80$ ms, the impact of N_{SS} on the PHY layer performance is negligible, especially if the UE is in a LoS condition, where the SNR remains high. In the second phase, when the UE enters a NLoS condition, the SNR decreases in both cases.

Fig.5.6 is depicts a scenario in which $T_{SS} = 160$, and the antenna elements of the BS are 64. The comparison between $N_{SS} = 16$ and $N_{SS} = 32$ shows a different behaviour with respect to Fig.5.5. In fact, increasing the number of antenna elements, the impact of N_{SS} becomes more evident for both the LoS and the NLoS conditions. Also in this case, when the UE enters a NLoS condition, the SNR decreases for both models.

Finally, we report in Fig.5.7 the results obtained when deploying a gNB featuring the 16 antenna array configuration, $N_{SS} = 32$, and $T_{SS} = \{80,160\}$ ms. In this way it is possible to see the role of T_{SS}. As shown in Fig.5.7 when the burst period increases the SNR does not deteriorate, especially in LoS. In the second phase, when the UE enters a NLoS condition, the SNR decreases,as in previous cases, but the trend of the analyzed configurations remains similar.

5.2.2 Application level performance

The second part of the simulations focuses on the end-to-end performance of the system. For this analysis, we install an UDP client-server pair on the gNB and the UE. Then, we extract metrics such as latency, throughput, and the packet drop rate (PDR). The parameters

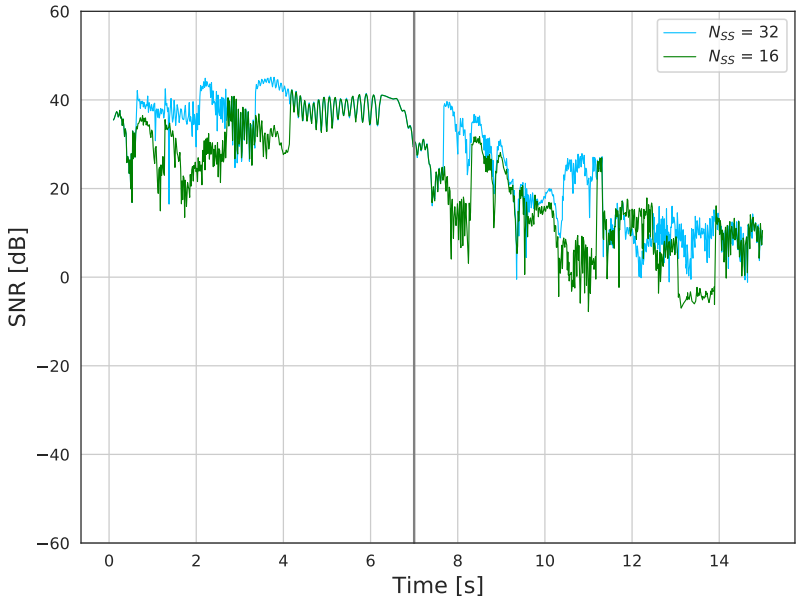

Figure 5.6: SNR vs time for number of antennas at BS = 64, T_{SS} = 160 ms, N_{SS} = {32,16}. The black vertical line represents the time instant during which the UE ends up in a NLoS condition.

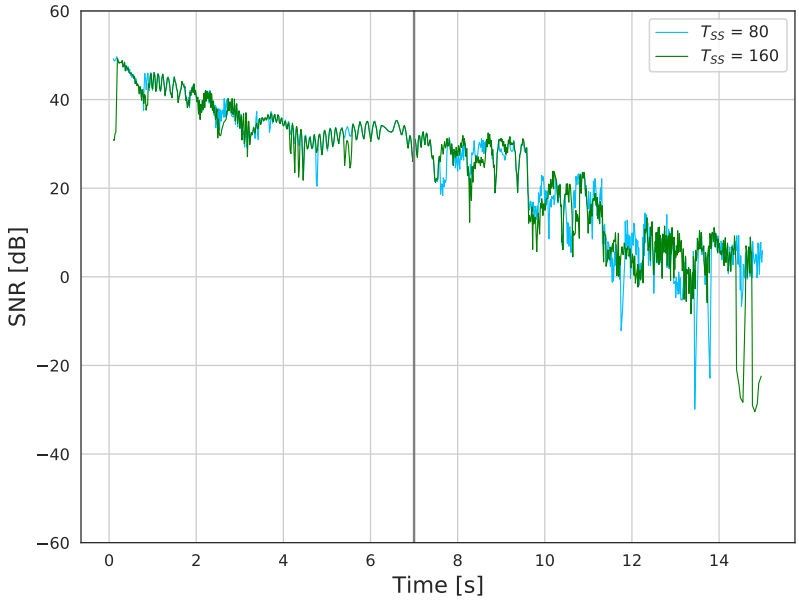

Figure 5.7: SNR vs time for number of antennas at BS = 16, N_{SS} = 32, T_{SS} = {80,160} ms. The black vertical line represents the time instant during which the UE ends up in a NLoS condition.

are set in order to ensure appreciable results, therefore the number of antenna elements at the BS is very low, set to 4, while all the possible combinations for the other parameters, such as N_{SS} and T_{SS}, are considered. The following results are obtained averaging the outcomes of 20 simulations.

The first analyzed metric is the latency, whose results are visible in Fig.5.8.

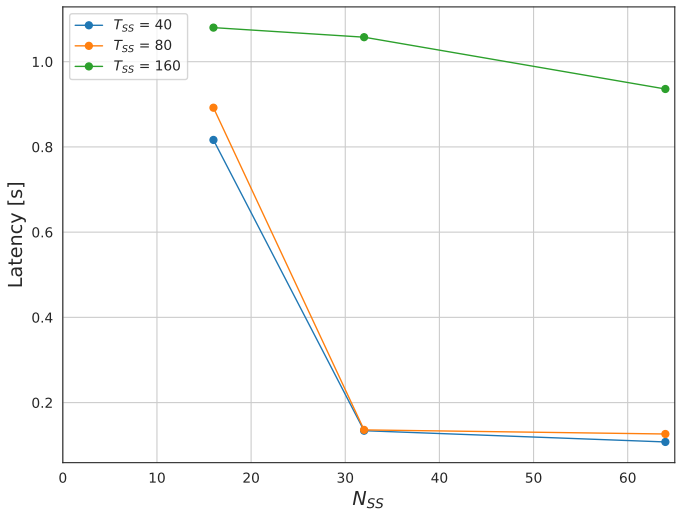

Figure 5.8: Average latency for 4 antenna elements at the gNB and different beam management configurations.

In this case there is a pronounced difference between the latency obtained setting $T_{SS} = 160$, and those with $T_{SS} = 80$ or $T_{SS} = 40$, meaning that lower T_{SS} leads to lower latency. This enhances the role of the burst period, in particular if the number of antenna elements at BS is really low. Moreover, also increasing the N_{SS} results in lower latency, especially the step from $N_{SS} = 16$ to $N_{SS} = 32$ greatly reduces the latency for $T_{SS} = \{40,80\}$ ms, while the difference between $N_{SS} = 32$ and $N_{SS} = 64$ is not significant.

Then, we considered the APP layer throughput, defined as the amount of data that is successfully received over the communication link, and whose results are visible in Fig.5.9. Analogous to the pre-

viously example, the difference between the cases with $T_{SS} = 40$ ms and $T_{SS} = 80$ ms, with the case where $T_{SS} = 160$ ms, is really pronounced, in particular lower T_{SS} leads to higher throughput. Taking as an example $N_{SS} = 32$, we obtain a throughput of 1.25 MB/s for $T_{SS} = 160$ ms, while increases up to 1.329 and 1.333 MB/s for $T_{SS} = \{80,40\}$ ms respectively. The incidence of N_{SS} is marked in the step between $N_{SS} = 16$ and $N_{SS} = 32$, especially for $T_{SS} = \{40,80\}$ ms, while is more moderate for $T_{SS} = 160$ ms.

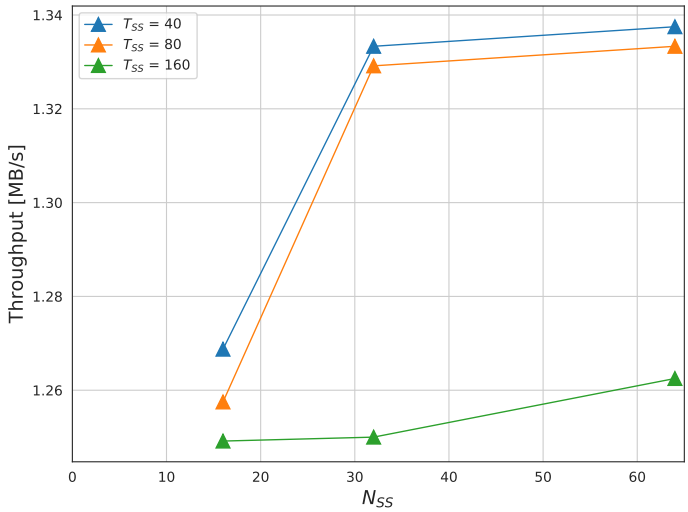

Figure 5.9: Average throughput for 4 antenna elements at the gNB and different beam management configurations.

Finally we present the PDR, which represents the number of packets lost or dropped during the transmission. This metric must be kept low in order to guarantee certain data rates. In a transmission interval, the PLR can be calculated as follows:

$$PLR = \frac{N^{tx} - N^{rx}}{N^{tx}} \times 100\% \tag{5.1}$$

where N^{tx} and N^{rx} are the total number of transmitted and received packets, respectively. This evaluation can be easily performed by extracting all the real-time packet sizes which are both transmitted

and received respectively.

In this case the results, depicted in Fig.5.10, are comparable to those previously discussed for latency, shown in Fig.5.8.

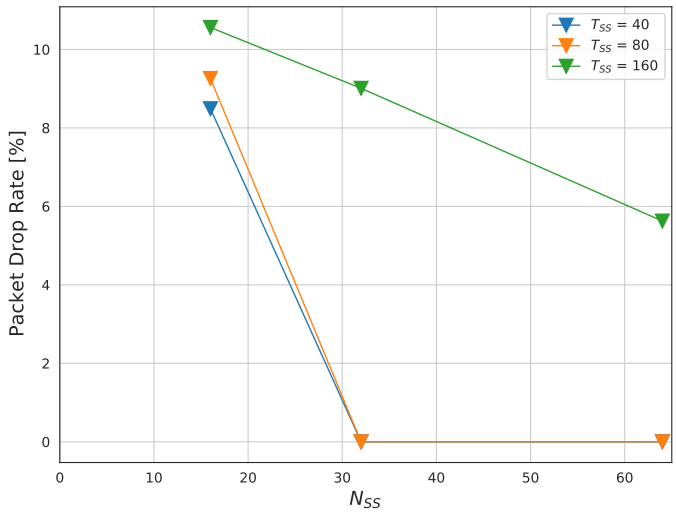

Figure 5.10: Average PDR for 4 antenna elements at the gNB and different beam management configurations.

For $T_{SS} = 40$ ms and $T_{SS} = 80$ ms the results are really similar for $N_{SS} = 16$, where the percentage of PDR is around 9%, and are equal for $N_{SS} = 32$ and 64, where no packets are dropped. This enhances the role of N_{SS} for array configurations featuring fewer radiating elements, since the PDR is nullified increasing the N_{SS}. For $T_{SS} = 160$ ms the impact of N_{SS} is less dramatic. Even though the PDR decreases with respect to an increase of N_{SS}, a residual PDR can be noticed also for $N_{SS} = 64$. This suggests that the periodicity considered can not support the traffic demands, regardless of the value of N_{SS}.

Chapter 6

Conclusion and future works

This thesis proposed a realistic implementation of DL beam management procedure, where the choice of the beams is based on the SS blocks, which are periodically exchanged between the transmitter and the receiver nodes.

Specifically, a brief summary of the 5G technology is provided, featuring a detailed description of the NR access technology, where we explored the frame structure, the scheduling, and the IA. Moreover, mmWave frequencies are explained, highlighting propagation characteristics and their role on system design. Then, the architecture of the beamforming is described, along with beam management procedures, distinguishing in particular between the idle- mode beam management and the connected-mode beam management. After the description of ns-3 simulator as the designated simulation framework, the main contributions of this thesis are analyzed. Specifically, we explained how the ns-3 code base was extended with additional modules and methods to simulate beam management according to 3GPP NR specifications, including detailed SS-block-based implementation of initial access. Then, we described different scenarios to compare the performance of different beam management configurations as a function of several metrics.

Results show that increasing the number of SS blocks per burst

(N_{SS}) and decreasing the inter-burst periodicity (T_{SS}) increase the SNR, especially if the UE is in a LoS condition. Also the number of antenna elements in the BS affects the performance, since more antennas imply higher SNR and less linear behaviour.

Regarding the application metrics we considered a configuration with few antenna elements at the BS (i.e. 4 antenna elements) in order to enhance the results by reducing the search space for beam management . Specifically, more N_{SS} decreases the latency and the packet drop rate, while increasing the throughput. For T_{SS} metric the behaviour is the opposite, since longer T_{SS} leads to higher latency and packet drop rate, while the throughput becomes lower.

As a part of future works, to improve the ns-3 module and add functionalities that make the framework more realistic and complete, we will design the UL beam management through the implementation of SRSs, that are used to monitor the uplink channel quality. In this case, a pool of uplink SRS resources are transmitted by UE corresponding to different analog beams. Beam selection operation is done at BS side, while beam measurement results from uplink SRS can be applied to beam selection for downlink analog beams based on channel reciprocity in spatial domain [53].

Another improvement for the DL beam management procedure can be given by the implementation of CSI-RSs, which is used for Radio Resource Management (RRM) measurements for mobility management purposes in connected mode. In this case the beam selection is done at the UE side, and it will be reported to BS.

Finally, as part of our future work, the use of Artificial Intelligence (AI) including machine learning (ML) algorithms, to improve the beam management procedures in the following two aspects:

- mitigate the complexity of radio resource management problem, where a deep-learning-based beam management and interference coordination is proposed [54];

- improve beam tracking implementing a ML solution, which is proposed to enhance beam management and UEs' scheduling by modeling the mapping between geo-locations of UEs and their serving beams or serving cells [55].

Bibliography

[1] Siddiqi, Murtaza and Yu, Xinjun and Joung, *5G Ultra-Reliable Low-Latency Communication Implementation Challenges and Operational Issues with IoT Devices*, Electronics, vol. 8, pp.981, September 2019.

[2] ITU,https://www.itu.int/en/ITU-R/study-groups/rsg5/rwp5d/imt-2020/Pages/default.aspx

[3] Patrick Kwadwo Agyapong, Mikio Iwamura, Dirk Staehle, Wolfgang Kiess, Anass Benjebbour. *Design Considerations for a 5G Network Architecture*, IEEE Communications Magazine, vol. 52, no. 11, pp. 65-75, November 2014.

[4] Yunman Hao, *Investigation and Technological Comparison of 4G and 5G Networks*, Journal of Computer and Communications, vol. 9, pp.36-43, 2021.

[5] D. Wang, D. Chen, B. Song, N. Guizani, X. Yu and X. Du. *From IoT to 5G I-IoT: The Next Generation IoT-Based Intelligent Algorithms and 5G Technologies*, IEEE Communications Magazine, vol. 56, no. 10, pp. 114-120, October 2018.

[6] Murtaza Ahmed Siddiqi, Heejung Yu, Jingon Joung. *Millimeter-wave beamforming as an enabling technology for 5G cellular communications: theoretical feasibility and prototype results*, Electronics, 2019.

[7] W. El-Beaino, A. M. El-Hajj and Z. Dawy. *On Radio network planning for next generation 5G networks: A case study* 2015 International Conference on Communications, Signal Processing, and their Applications (ICCSPA'15), pp. 1-6, 2015.

[8] Marco Giordani, Michele Polese, Arnab Roy, Douglas Castor, Michele Zorzi. *A Tutorial on Beam Management for 3GPP NR at mmWave Frequencies*, IEEE Communications Surveys Tutorials, vol. 21, no. 1, pp. 173-196, 2019.

[9] 3GPP, https://www.3gpp.org/about-3gpp/about-3gpp

[10] Ns-3, https://www.nsnam.org

[11] Gkonis Panagiotis, Panagiotis Trakadas, Kaklamani Dimitra. *A Comprehensive Study on Simulation Techniques for 5G Networks: State of the Art Results, Analysis, and Future Challenges*, Electronics, vol. 9, pp. 468, March 2020.

[12] Ramije Zeqiri, Florim Idrizi, Halim Halimi. *Comparison of Algorithms and Technologies 2G, 3G, 4G and 5G*, 2019 3rd International Symposium on Multidisciplinary Studies and Innovative Technologies (ISMSIT), pp. 1-4, 2019.

[13] Anutusha Dogra, Rakesh Kumar Jha, Shuba Jain. *A Survey on Beyond 5G Network With the Advent of 6G: Architecture and Emerging Technologies*, IEEE Access, vol. 9, pp. 67512-67547, October 2021.

[14] Stefan Parkvall, Erik Dahlman, Anders Furuskar, Mattias Frenne. *NR – The new 5G radio-access technology*, IEEE Communications Standards Magazine, vol. 1, no. 4, pp. 24-30, December 2017.

[15] Balazs Bertenyi, Satoshi Nagata, Havish Kooropaty, Xutao Zhou, Wanshi Chen, Younsun Kim, Xizeng Dai, Xiaodong Xu. *5G NR Radio Interface*, J. ICT Stand., vol. 6, pp. 31-58, May 2018.

[16] Lin Xingqin, Li Jingya, Baldemair Robert, Cheng Thomas, Parkvall Stefan, Larsson Daniel, Koorapaty Havish, Frenne Mattias, Falahati Sorour, Grövlen Asbjörn, Werner Karl. *5G New Radio: Unveiling the Essentials of the Next Generation Wireless Access Technology*, IEEE Communications Standards Magazine, vol. 3, no. 3, pp. 30-37, September 2019.

[17] Yong Niu, Yong Li, Depeng Jin, Li Su, Athanasios V. Vasilakos. *A survey of millimeter wave communications (mmWave) for 5G: opportunities and challenges*, Wireless Networks, vol. 21, February 2015.

[18] Mothana L. Attiah, Azmi Awang Md Isa, Zahriladha Zakaria, M. K. Abdulhameed, Mowafak K. Mohsen, Ihab A. Ali. *A survey of mmWave user association mechanisms and spectrum sharing approaches: an overview, open issues and challenges, future research trends*, Wireless Networks, vol. 26, pp. 2487-2514, May 2020.

[19] Zhao Qingling, Jin Li. *Rain Attenuation in Millimeter Wave Ranges*, 2006 7th International Symposium on Antennas, Propagation EM Theory, pp. 1-4, 2006.

[20] W. El-Beaino, A. M. El-Hajj, Z. Dawy. *On Radio network planning for next generation 5G networks: A case study*, 2015 International Conference on Communications, Signal Processing, and their Applications (ICCSPA'15), pp. 1-6, 2015.

[21] C. Seker, M. T. Güneser, T. Ozturk. *A Review of Millimeter Wave Communication for 5G*, 2018 2nd International Sympo-

sium on Multidisciplinary Studies and Innovative Technologies (ISMSIT), pp. 1-5, 2018.

[22] S. Singh, F. Ziliotto, U. Madhow, E. Belding, M. Rodwell. *Blockage and directivity in 60 GHz wireless personal area networks: from cross-layer model to multihop MAC design*, IEEE Journal on Selected Areas in Communications, vol. 27, no. 8, pp. 1400-1413, October 2009.

[23] S. Collonge, G. Zaharia, G. E. Zein. *Influence of the human activity on wide-band characteristics of the 60 GHz indoor radio channel*, IEEE Transactions on Wireless Communications, vol. 3, no. 6, pp. 2396-2406, Nov. 2004.

[24] Z. Genc, U. H. Rizvi, E. Onur, I. Niemegeers. *Robust 60 GHz Indoor Connectivity: Is It Possible with Reflections?*, 2010 IEEE 71st Vehicular Technology Conference, pp. 1-5, 2010.

[25] Xueli An, Chin-Sean Sum, R. Venkatesha Prasad, Junyi Wang, Zhou Lan, Jing Wang, Ramin Hekmat, Hiroshi Harada, Ignas Niemegeers. *Beam switching support to resolve link blockage problem in 60 GHz WPANs*, 2009 IEEE 20th International Symposium on Personal, Indoor and Mobile Radio Communications, pp. 390-394, 2009.

[26] Russell Ford, Menglei Zhang, Sourjya Dutta, Marco Mezzavilla, Sundeep Rangan, Michele Zorzi. *A Framework for End-to-End Evaluation of 5G mmWave Cellular Networks in ns-3*, Workshop on ns3, pp. 85-92, June 2016.

[27] M. Park, H. K. Pan. *A Spatial Diversity Technique for IEEE 802.11ad WLAN in 60 GHz Band*, IEEE Communications Letters, vol. 16, no. 8, pp. 1260-1262, August 2012.

[28] Soodabeh Darzi, Tiong Sieh Kiong, Mohammad Tariqul Islam, Mahamod Ismail, Salehin Kibria, Balasem Salem. *Null Steering of Adaptive Beamforming Using Linear Constraint Minimum Variance Assisted by Particle Swarm Optimization, Dynamic Mutated Artificial Immune System, and Gravitational Search Algorithm*, The Scientific World Journal, vol. 2014, no. 5,July 2019.

[29] Mohamed Nadder Hamdy. *White paper beamformer explained*, CommScope White Papers, 19 August 2020.

[30] Analogictips, https://www.analogictips.com/mmwave-antennas-and-antenna-management-for-5g/ (accessed March 2022)

[31] Koc Asil, Masmoudi Ahmed and Le-Ngoc Tho. *Full-Duplex Non-Coherent Communications for Massive MIMO Systems with Analog Beamforming*, ICC 2022 - IEEE International Conference on Communications, pp. 4667-4672 , 2022.

[32] David Borges, Paulo Montezuma, Rui Dinis, Marko Beko. *Massive MIMO Techniques for 5G and Beyond—Opportunities and Challenges*, Electronics, vo.10, no.14, 2021.

[33] Al-Hubaishi Ahme, Noordin Nor, Sali Aduwati, Subramaniam, Shamala, Mansoor Ali. *An Efficient Pilot Assignment Scheme for Addressing Pilot Contamination in Multicell Massive MIMO Systems*, Electronics, vo.8, March 2019.

[34] *Measurement configuration and reporting considering additional RS*, Huawei - Tdoc R2-1703387, 2017.

[35] 3GPP. *NR and NG-RAN Overall Description - Rel. 15*, TS 38.300, 2018.

[36] *NR PRACH preamble resource allocation* Ericsson - Tdoc R1-1611905, 2016.

[37] *Measurement configuration for CSI-RS*, Ericsson - Tdoc R2-1704103, 2017.

[38] , *NR - Radio Resource Control (RRC) protocol specification - Release 15* TS 38.331, 2018.

[39] 3GPP. *NR - Physical channels and modulation - Release 15*, TS 38.211, V15.0.0, 2018.

[40] *Consideration on CSI RS for beam management* ZTE Corporation - Tdoc R2-1708123, 2017.

[41] Marco Mezzavilla, Menglei Zhang, Michele Polese, Russell Ford, Sourjya Dutta, Sundeep Rangan, Michele Zorzi. *End-to-End Simulation of 5G mmWave Networks*, IEEE Communications Surveys Tutorials, vol. 20, no. 3, pp. 2237-2263, 2018.

[42] T. Levanen, J. Pirskanen and M. Valkama. *Radio interface design for ultra-low latency millimeter-wave communications in 5G Era*, 2014 IEEE Globecom Workshops (GC Wkshps), pp. 1420-1426, 2014.

[43] S. Dutta, M. Mezzavilla, R. Ford, M. Zhang, S. Rangan, M. Zorzi. *MAC layer frame design for millimeter wave cellular system*, 2016 European Conference on Networks and Communications (EuCNC), pp. 117-121, 2016.

[44] Zhang Menglei, Polese Michele, Mezzavilla Marco, Rangan Sundeep, Zorzi Michele. *Ns-3 Implementation of the 3GPP MIMO Channel Model for Frequency Spectrum above 6 GHz*, pp. 71-78, 2017.

[45] H.Dembele, M. L. Bot, F. Gallee, P. Pajusco. *Impact of Human Blockage on 5G Communication System in the 26 GHz Band*, 2021 15th European Conference on Antennas and Propagation (EuCAP), pp.1-5, 2021.

[46] Mezzavilla Marco, Dutta Sourjya, Zhang Menglei, Akdeniz Mustafa, Rangan Sundeep. *5G mmWave Module for ns-3 Network Simulator*, (2015).

[47] D. J. Love, R. W. Heath. *Equal gain transmission in multiple-input multiple-output wireless systems*, IEEE Transactions on Communications, vol. 51, no. 7, pp. 1102-1110, July 2003.

[48] M. Rebato, M. Mezzavilla, S. Rangan, F. Boccardi and M. Zorzi. *Understanding Noise and Interference Regimes in 5G Millimeter-Wave Cellular Networks*, European Wireless 2016; 22th European Wireless Conference, pp. 1-5, 2016.

[49] Ghosh Amitava, Thomas Timothy A., Cudak Mark C., Ratasuk Rapeepat, Moorut Prakash, Vook Frederick W., Rappaport Theodore S., MacCartney George R., Sun Shu, Nie Shuai. *Millimeter-Wave Enhanced Local Area Systems: A High-Data-Rate Approach for Future Wireless Networks*, IEEE Journal on Selected Areas in Communications, vol. 32, no. 6, pp. 1152-1163, 2014.

[50] Pi Zhouyue, Khan Farooq. *System design and network architecture for a millimeter-wave mobile broadband (MMB) system*, 34th IEEE Sarnoff Symposium, pp. 1-6, 2011.

[51] M. Cudak, T. Kovarik, T. A. Thomas, A. Ghosh, Y. Kishiyama, T. Nakamura. *Experimental mm wave 5G cellular system*, 2014 IEEE Globecom Workshops (GC Wkshps)2014 IEEE Globecom Workshops (GC Wkshps), pp. 377-381, 2014.

[52] Mattia Lecci, Paolo Testolina, Marco Giordani, Michele Polese, Tanguy Ropitault, Camillo Gentile, Neeraj Varshney, Anuraag Bodi, Michele Zorzi. *Simplified Ray Tracing for the Millimeter Wave Channel: A Performance Evaluation*, 2020 Information Theory and Applications Workshop (ITA), pp. 1-6, 2020.

[53] Y. N. R. Li, B. Gao, X. Zhang and K. Huang. *Beam Management in Millimeter-Wave Communications for 5G and Beyond*, IEEE Access, vol. 8, pp. 13282-13293, 2020.

[54] P. Zhou, X. Fang, X. Wang, Y. Long, R. He and X. Han. *Deep Learning-Based Beam Management and Interference Coordination in Dense mmWave Networks*, IEEE Transactions on Vehicular Technology, vol. 68, no. 1, pp. 592-603, January 2019.

[55] M. Arvinte, M. Tavares and D. Samardzija. *Beam Management in 5G NR using Geolocation Side Information*, 2019 53rd Annual Conference on Information Sciences and Systems (CISS), pp. 1-6, 2019.

Acknowledgements

First of all, I want to thank my parents, they do not make me miss anything and they constantly support me. I would like to thank my sisters, for the patience and the ongoing suggestions.

I would like to express my sincere gratitude to my thesis supervisor Prof. Michele Zorzi, and to co-supervisor Prof. Marco Giordani and Matteo Pagin, for their assistance at every stage of this thesis. Your help has been essential for my work.

I would like to thank all my friends who have shared with me these years, Luca, Mari, Laura, and Ari, for the great time spent together.

Finally, I have to be grateful to my colleagues for their help and comprehension, Federica, Simone, Ludovica, Alberto, and Rosario.